Nano Research

Open Access

Research Article

Prebiotic-based "Shield" hydrogel embedded with rod-shaped Mn_2(Olsa) MOF particles for inflammatory bowel disease and associated mental disorders

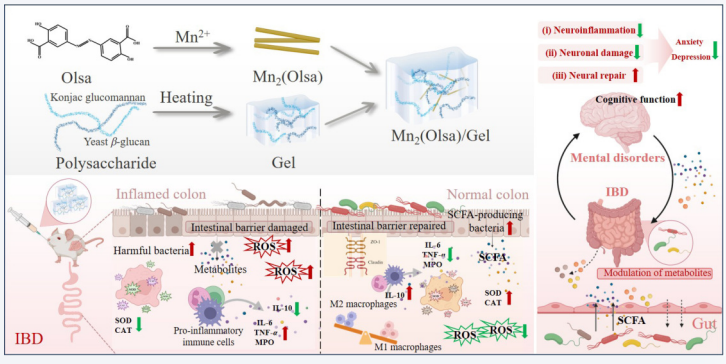
Xiaozhen Wang[1], Wenya Su[1], Xia Li[1] ✉, Han Xu[1], Hongyue Tian[1], Luqi Huang[2], Lanping Guo[2] ✉, and Wenyuan Gao[1] ✉

[1] *Tianjin Key Laboratory for Modern Drug Delivery & High-Efficiency, School of Pharmaceutical Science and Technology, Faculty of Medicine, Tianjin University, Tianjin 300193, China*

[2] *National Resource Center for Chinese Materia Medica, Academy of Chinese Medical Sciences, China State Key Laboratory for Quality Ensurance and Sustainable Use of Dao-di Herbs, Beijing 100700, China*

Cite this article: *Nano Research*, **2026**, *19*, 94908754. https://doi.org/10.26599/NR.2026.94908754

ABSTRACT: Inflammatory bowel disease (IBD), with its colonic predilection, was frequently complicated by neuropsychiatric comorbidities such as anxiety and depression. To address this, we developed a colon-targeted, prebiotic-based synergistic therapeutic system. This system integrated anti-inflammatory and antioxidative rod-shaped Mn_2(Olsa) metal-organic framework (MOF) particles with a yeast *β*-glucan/konjac glucomannan (YG/KGM) composite gel designed to remodel the gut microenvironment. The resulting Mn_2(Olsa)/Gel composite ensured sustained intestinal adhesion and retention, facilitating efficient colon-targeted delivery. It effectively alleviated hallmark pathologies of IBD, including intestinal inflammation, microbial dysbiosis, barrier disruption, oxidative stress, and immune imbalance. In addition, the treatment significantly mitigated IBD associated anxiety- and depression-like behaviors. This work establishes a novel, targeted paradigm for the combined management of IBD and its neuropsychiatric comorbidities.



KEYWORDS: inflammatory bowel disease, hydrogel, colon-targeted delivery, anxiety-like and depression-like behaviors

1 Introduction

Inflammatory bowel disease (IBD) (including Crohn's disease and ulcerative colitis) remains a challenging clinical problem due to its complex pathological features (e.g., oxidative stress damage, disturbances in gut microbiota, and disruption of the intestinal barrier). Its clinical management is also difficult because it is a progressive, chronic disease, and many patients suffer from recurrent flare-ups and fail to achieve optimal disease control [1].

Currently, the main drugs used in the treatment of IBD include immunosuppressants, glucocorticoids and anti-inflammatory drugs, which aim to alleviate the symptoms and reduce the immune response. However, these drugs are not able to target the lesions, and their long-term use can lead to serious side effects such as hepatotoxicity, allergic reactions and gastrointestinal discomfort [2–4]. This underscores an imperative to engineer colon- and inflammation-specific drug delivery systems that maximize local efficacy while circumventing systemic toxicities [5, 6].

IBD comorbidities (especially psychiatric disorders) have gained attention with the increasing understanding of IBD. Compared to the general population, patients with IBD are more likely to develop mental disorders such as anxiety and depression, which in turn reduces the quality of life of IBD patients. Studies have shown that about 32.1% of IBD patients have anxiety symptoms and 25.2% have depressive symptoms [7]. The bidirectional relationship between IBD and its associated psychiatric disorders of depression and anxiety may be manipulated by the intricate communication between the gut and the brain (familiarly known as the gut-brain axis (GBA)), with mechanisms behind the crosstalk including

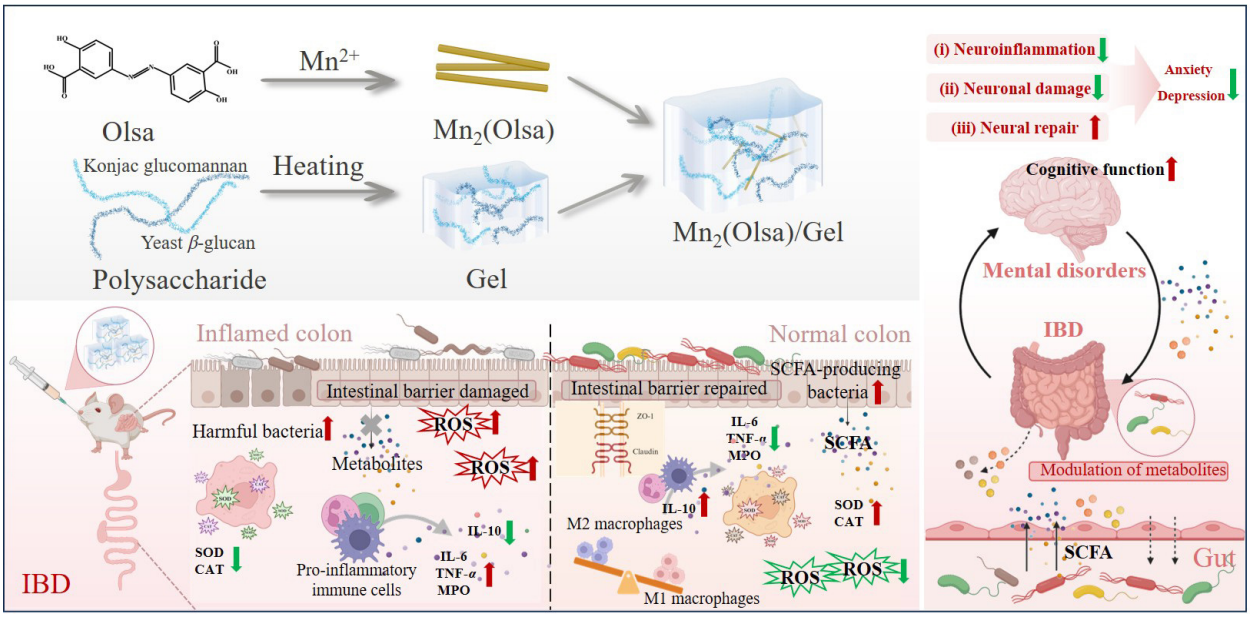
Received: January 15, 2026; **Revised:** April 20, 2026
Accepted: April 20, 2026

✉Address correspondence to Xia Li, lixia2008@tju.edu.cn; Lanping Guo, glp01@126.com; Wenyuan Gao, pharmgao@tju.edu.cn

dysbiosis of gut microbiota, increased pro-inflammatory cytokines, as well as immune and endocrine disruption [8]. Although recent studies have explored the potential impact of antidepressants or specific medications for IBD on the therapeutic management of IBD patients with psychiatric co-morbidities, their findings remain unclear [9]. Therefore, intervention strategies are necessary to alleviate IBD and its associated depressive and anxiety co-morbidities. In contrast to the study previously [10], our research focuses on the comorbidity mechanisms of IBD with anxiety and depression. Addressing the critical clinical challenge where 32.1% of IBD patients experience anxiety and 25.2% suffer from depression, we propose a therapeutic goal of simultaneous intervention targeting both "intestinal pathology and neuropsychiatric symptoms", thereby transcending the traditional limitation of focusing solely on intestinal inflammation.

Targeted drug delivery systems with prebiotic carbohydrate have been used as promising means of IBD management due to favorable biocompatibility and colonic targeting properties [11]. Compared with intravenous injection, intraperitoneal injection, and colonic administration, oral administration is more convenient, safer, and more compliant for patients in the treatment of intestinal diseases. However, the acidic environment of the gastrointestinal tract can lead to rapid drug degradation, thereby affecting the drug's efficacy [12]. Based on the natural digestive properties of plant-derived polysaccharide prebiotics, certain polysaccharides cannot be degraded in the upper gastrointestinal tract, but can only enter the colon directly and be degraded as a "substrate" for the gut microbiota, thus generating biologically active metabolites and exerting their multiple regulatory effects. Yeast β-glucan (YG) is a bioactive polysaccharide extracted from yeast cell walls [13], and was recognized by the U.S. Food and Drug Administration (FDA) in 2009 as a Generally Recognized as Safe (GRAS) substance for use in dietary supplements and functional foods. In addition, it is specifically recognized by receptors (e.g., Dectin-1) on the surface of immune cells (macrophages, dendritic cells), thus exerting its powerful immunomodulatory effects. In particular, it has been demonstrated that YG attenuated colitis by regulating gut microbiota, promoting short-chain fatty acid (SCFA) production and modulating the interleukin-17 (IL-17) signaling pathway [14]. Meanwhile, it has been shown to improve neuroinflammation and cognitive deficits associated with a number of diseases [15] and has potential for the treatment of IBD and its associated psychiatric disorders [16]. Konjac glucomannan (KGM) is a functional polysaccharide extracted from *Amorphophallus konjac* C. Koch and is known for its excellent gel-forming ability [17]. However, single-component hydrogels are often limited by poor mechanical properties, including low flexibility and high brittleness [18]. To address this, we developed a novel composite hydrogel that departs from previously reported inulin-only based gel [10]. Our formulation integrates YG with KGM, leveraging YG's potential immunomodulatory and neuroprotective bioactivity alongside KGM's superior gelation capacity. The resultant dual-network matrix demonstrates markedly enhanced flexibility and bioadhesion, thereby overcoming the brittleness and functional monotony characteristic of mono-polysaccharide-based platforms.

Herein, we engineered a multifunctional prebiotic-based hydrogel system (YG@KGM) embedded with rod-shaped Mn_2(Olsa) metal-organic framework (MOF) particles (Scheme 1). Olsalazine, a clinical mainstay for IBD therapy, can be used as an organic linker capable of coordinating with abundant transition metals (e.g., Ru, Ce, Mn, Cu) to construct MOFs [10]. This coordination synergistically enhances the drug's aqueous solubility and bioactivity while augmenting its reactive oxygen species (ROS)-scavenging capacity due to the inherent properties of the transition ions. Notably, we pioneered the synthesis of Mn_2(Olsa) as a novel MOF derivative. To address dual challenges of limited colonic targeting and microbiota dysregulation inherent in Mn_2(Olsa), we synthesized a prebiotic-functionalized hydrogel composite (YG@KGM). This design synergistically: (i) augments site-specific drug delivery through enhanced mucosal adhesion; (ii) harnesses prebiotic-mediated gut microbiota remodeling and beneficial metabolite production to potentiate neuropsychiatric benefits. Critically, the Mn_2(Olsa)/Gel system enables spatiotemporally controlled drug delivery to the colon while orchestrating a multiple



Scheme 1 A schematic diagram illustrating the colon-targeted multifunctional therapeutic Mn_2(Olsa)/Gel and its potential mechanism in modulating dextran sulfate sodium (DSS)-induced IBD and its associated depression and anxiety.

therapeutic response: (i) attenuating intestinal inflammation; (ii) re-establishing epithelial barrier integrity; (iii) neutralizing oxidative stress; (iv) restoring gut microbiota homeostasis; and (v) modulating the immune response. The primary goal of the present study was to design and validate a multimodal synergistic system integrating ROS scavenging, anti-inflammatory activity, and gut microbiota modulation. While prior Olsa-based platforms such as the Cu_2(Olsa)/inulin hydrogel have established efficacy in IBD therapy and microbiota regulation [10], the therapeutic potential of these systems for neuropsychiatric comorbidities remains unexplored. Here, we demonstrate that our Mn_2(Olsa)/YG@KGM hydrogel addresses this gap through a multi-faceted mechanism. Integrating multi-omics analyses (16S ribosomal RNA (16S rRNA) sequencing, untargeted metabolomics, and SCFA quantification), we show that beyond ameliorating colitis, our system alleviates IBD-associated anxiety and depression by remodeling microbial metabolite profiles, suppressing neuroinflammation, and promoting hippocampal neuroplasticity. Collectively, this study provides a comprehensive investigation of both the intestinal pathophysiological changes and the neuropsychiatric sequelae in patients with IBD.

2 Experimental

2.1 Materials

Olsalazine sodium (purity ≥ 99%) and KGM were purchased from Aladdin Biochemical Technology Co., Ltd. (Shanghai, China). YG was obtained from Anhui Runtai Biotechnology Co., Ltd. (Anhui, China). Manganese chloride tetrahydrate ($MnCl_2·4H_2O$, 99.99% purity), 2,2'-azino-bis (3-ethylbenzothiazoline-6-sulfonic acid) diammonium salt (ABTS), H_2O_2 (analytic pure) and 4,4'-dioxido-3,3'-biphenyldicarboxylate (dobp, purity ≥ 97%) were obtained from Macklin (Shanghai, China). Enzyme-linked immunosorbent assay (ELISA) kits for tumor necrosis factor-alpha (TNF-α), interleukin-6 (IL-6), and interleukin-10 (IL-10) were purchased from Enzyme Linked Biotechnology Co., Ltd. (Shanghai, China). Lipopolysaccharide (LPS) and 1,1-diphenyl-2-picrylhydrazyl radical (DPPH), dichlorodihydrofluorescein diacetate (DCFH-DA) probe assay kit, the superoxide dismutase (SOD) assay kit, catalase (CAT) activity assay kit, myeloperoxidase (MPO) activity assay kit, and mitochondrial membrane potential assay kit with JC-1 were obtained from Beijing Soleibao Technology Co., Ltd. (Beijing, China). Cell counting kit-8 (CCK-8) and the annexin V-FITC apoptosis detection kits were obtained from Beyotime Institute of Biotechnology (Shanghai, China). Calcein AM/PI double staining kit was supplied by Elabscience Biotechnology Co., Ltd. (Wuhan, China). Aspartate aminotransferase (AST) assay kit, alanine transaminase (ALT) assay kit, blood urea nitrogen (BUN) assay kit, and creatinine (Cre) assay kit were purchased from yuanye Bio-Technology Co., Ltd. (Shanghai, China).

2.2 Synthesis of Mn_2(Olsa) MOF

A 20 mM solution of $MnCl_2$ (50 mL) was added dropwise to a 10 mM solution of olsalazine sodium (50 mL) at a rate of 1 mL/min. The mixture was heated at 20, 40, 60, 80 or 100 °C for 12 h. The precipitate was then centrifuged and washed three times with distilled water to obtain Mn_2(Olsa). Subsequently, Mn_2(Olsa) was prepared by varying the Mn/Olsa ratio and time to obtain the optimal preparation conditions. The dose of Olsa in the supernatant (C_1) was determined, and the yield of MOF was calculated by the following formula: yield (%) = $(C_0 - C_1)/C_0 \times 100$, C_0: initial Olsa dose.

2.3 Synthesis of Mn_2(Olsa)/Gel

The preparation of the composite hydrogel is the same as before, with slight modifications [19]. Briefly, the YG powder (400 mg) was hydrated in distilled water and stirred at 80 °C for 30 min, followed by the addition of 5% (w/v) KGM stock solution mixed with the YG stock solution, and incubated with Mn_2(Olsa) and 0.5% (w/v) Na_2CO_3 for 10 min. Finally, all samples were cooled at room temperature overnight to obtain Mn_2(Olsa)/Gel. Mn_2(dobp)/Gel and Olsa/gel were similarly prepared.

2.4 Characterizations

The morphology and elemental distribution were recorded using a scanning electron microscope (SEM, SU3500, Hitachi Ltd, Tokyo, Japan), a transmission electron microscope (TEM, TecnaiG2F20, Netherlands) and energy-dispersive X-ray spectroscopy (EDS). The element analysis and valence state of Mn on the surface of Mn_2(Olsa) was further analyzed by X-ray photoelectron spectroscopy (XPS, Thermo Fisher ESCALAB 250Xi, USA). The powder X-ray diffraction (PXRD) patterns were performed on the X-ray diffractometer (MiniFlex-600, Rigaku Corporation, Japan). The content of Mn element was determined via inductively coupled plasma optical emission spectrometry (ICP-OES) (ThermoICPOES7200, Thermo Fisher Scientific, USA). Rheological properties of Mn_2(Olsa)/Gel were determined by the HAAKE rheometer (MAR302, Anton Paar, Austria).

2.5 Gastrointestinal tract retention of Mn_2(Olsa)/Gel

Fluorescein isothiocyanate (FITC)-labeled YG was synthesized based on previous studies [20]. Briefly, YG (500 mg) was dissolved in 25 mL of purified water and the pH was adjusted to 8.0 with 0.5 mol/mL $NaHCO_3$ solution, followed by the addition of 25 mg of FITC. After stirring for 24 h at room temperature under light-avoidance conditions, anhydrous ethanol was added until the final concentration of ethanol was 80% (v/v). After centrifugation, the supernatant was discarded, the precipitate was re-dissolved with water, and the precipitate was washed repeatedly with anhydrous ethanol until there was no fluorescence absorption in the supernatant. After lyophilization of the precipitate, FITC-labeled YG was obtained. FITC-labeled YG gels were prepared by mixing unlabeled YG with FITC-labeled YG at a mass ratio of 5:1. The fluorescence images of mice gastrointestinal tract after gavage of FITC-labeled Mn_2(Olsa)/Gel or Gel for 1, 4, 12, and 24 h were obtained using the IVIS optical imaging system to study its retention in mice.

2.6 Evaluation of the anti-apoptotic and intracellular ROS scavenging activity of Mn_2(Olsa)

Raw264.7 cells were inoculated into 6-well plates and incubated at 37 °C for 24 h. Afterwards, the *in vitro* oxidative stress model was induced with H_2O_2 (5 mM). After 24 h, the medium was removed and the cells were treated with Mn_2(Olsa) (50 or 150 μg/mL) for 24 h. Cells were stained with Annexin V/PI or ROS probe DCFH-DA according to the instructions of the corresponding kits. Finally, apoptosis and intracellular ROS levels were assessed by flow cytometry (BD Biosciences, USA) and the data were analyzed by FlowJo software.

2.7 The protective effect of Mn_2(Olsa) on H_2O_2-induced oxidative damage

Raw264.7 cells and CT26 cells were inoculated into confocal Petri dishes, respectively. After 24 h of incubation, the medium was removed and each well was stimulated by adding H_2O_2 (5 mM) for 24 h, except for the blank wells, after which the modeling solution was removed and Mn_2(Olsa) (50 or 150 μg/mL) was added for the intervention for 24 h. For Live/Dead staining, the drug was incubated for 24 h, the medium was removed, and the Raw264.7 cells were obtained by 0.25% trypsin-EDTA digestion, followed by resuspension of the cells with a 1× assay buffer to resuspend the cells and stained for Calcein AM/PI according to previous literature method [21]. For JC-1 staining, the medium was removed after Mn_2(Olsa) (50 μg/mL or 150 μg/mL) incubation for 24 h, and then the Raw264.7 cells were reacted with JC-1 staining solution for 20 min at 37 °C. Subsequently, the supernatant was removed and the cells were washed twice with JC-1 staining buffer (1×) to remove the unbound dye, and finally, 1 mL of medium was added to each Petri dish and then visualized by a laser confocal microscope (Leica SP8, Germany).

2.8 *In vitro* anti-inflammatory activity of Mn_2(Olsa)

Raw264.7 cells were inoculated in 6-well plates at a density of 5×10^4. Each well was cultured for 24 h. Cells were treated with LPS (1 μg/mL) for 24 h, and Mn_2(Olsa) (50 or 150 μg/mL) was added for intervention for 24 h. The intracellular ROS level was detected by adding the ROS probe DCFH-DA, and was determined by confocal laser scanning microscopy (CLSM) and flow cytometry. For analysis of M1 and M2 surface marker expression, cells were stained with anti-CD86 and anti-CD206 antibodies for 30 min at 4 °C in the dark and then analyzed by flow cytometry. The levels of pro-inflammatory cytokines (TNF-α and IL-6) and anti-inflammatory cytokine (IL-10) in the supernatant were determined by ELISA kits in accordance with the manufacturer's instructions.

2.9 Therapeutic efficacy of Mn_2(Olsa)/Gel in DSS-induced acute colitis

Male C57BL/6 mice (6–8 weeks) were randomly divided into 6 groups and acute colitis was induced with 2.5% DSS (w/v) solution in drinking water for 6 days. Normal group (G1) was given sterile water without DSS and the rest of the groups were given freshly prepared DSS solution. All groups except the model group (G2) were treated by daily gavage Mn_2(dobp)/Gel (G3), Mn_2(Olsa)/Gel (G4), Olsa/Gel (G5) and Gel (G6) starting on the 5th day of DSS induction. During this period, the body weights of the mice were measured daily, while fecal blood and stool consistency were recorded to determine the disease activity index (DAI) (Table S1 in the ESM). The mice were subsequently euthanized, and the intestinal tissues were photographed and length determined. Colon tissues from each group of mice were collected, fixed in 4% paraformaldehyde, embedded in paraffin, and cut into 5 μm tissue sections for hematoxylin and eosin (H&E) staining (for assessing the morphology of colon tissues) and Alcian blue-periodic acid-Schiff (AB-PAS) staining (for assessing the goblet cells). Histological scoring of colon tissues was performed accordingly [22]. Mouse serum and mouse colon tissue were taken to detect inflammation-related cytokines (TNF-α, IL-6 and IL-10), MPO activity, and indicators of oxidative stress (SOD and CAT), all in strict accordance with the manufacturer's instructions. The levels of zonula occludens-1 (ZO-1) (1:5000, Servicebio) and Claudin-1 (1:3000, Servicebio) in intestinal tissues were measured by immunofluorescence to assess the protective effect of the Mn_2(Olsa)/Gel on the intestinal barrier, and the levels of inducible nitric oxide synthase (iNOS) (1:2000, Servicebio), M1 macrophage markers, and arginase-1 (Arg-1) (1:5000, Servicebio), M2 macrophage markers, respectively, were measured to assess the effect of the Mn_2(Olsa)/Gel on the regulation of intestinal immune homeostasis. The tissue sections were observed under a fluorescence microscope (NIKON ECLIPSE C1, Japan). Quantitative result analysis was conducted using ImageJ software.

2.10 Therapeutic efficacy of Mn_2(Olsa)/Gel in DSS-induced chronic colitis

Male C57BL/6 mice (6–8 weeks) were randomly divided into 6 groups: Normal group (G1), 1.5% DSS group (G2), 1.5% DSS + Olsa group (G3), 1.5% DSS + YG (G4), 1.5% DSS + Mn_2(Olsa)/Gel (G5) and 1.5% DSS + Gel (G6). They were first given 1.5% DSS (w/v) free drinking water for 6 consecutive days. During this period, drug intervention was carried out in different groups. Then, free drinking of sterile water was given for 6 consecutive days, and such cycle was repeated three times. During the 36-day continuous drug administration, body weight, fecal consistency and fecal blood were monitored and recorded. On the 37th day, all the mice were euthanized, and the serum, colon, and brain were collected for subsequent experiments. The major organs (heart, liver, spleen, lung, and kidneys) of G1 and G5 were collected, fixed in 4% paraformaldehyde, embedded in paraffin, and cut into 5 μm tissue sections for H&E staining. The levels of AST, ALT, BUN, and Cre in serum were measured. All animal experiments strictly adhered to the Guidelines for Care and Use of Laboratory Animals of the National Institutes of Health and were approved by the Zhongxin Huake (Tianjin) Biotechnology Co., Ltd., number ZXHK-DWLL-2025-0013. Humane endpoints were strictly implemented following institutional animal care guidelines. A loss of ≥ 20% of initial body weight was set as the predefined humane endpoint, and daily body weight monitoring was performed. No mice exceeded this threshold during the study, and all animals were maintained in accordance with ethical regulations.

2.11 Neuroprotective effects of Mn_2(Olsa)/Gel on IBD-induced anxiety and depression

At the end of the experiment, all mice were euthanized, and brain tissues were collected and fixed in 4% paraformaldehyde, partially used for Nissl staining and quantitative analysis of live neurons in the CA3 and DG regions. Immunofluorescence was used to label hippocampal astrocytes for glial fibrillary acidic protein (GFAP) (1:8000, Servicebio), microglia for ionized calcium-binding adapter molecule 1 (Iba1) (1:2000, Servicebio) for neuroinflammation assessment, and microtubule-associated protein 2 (MAP-2) (1:200, Servicebio) for brain tissue damage assessment. The tissue sections were observed under a fluorescence microscope. Quantitative result analysis was conducted using ImageJ software.

2.12 Microbiome analysis

The 16S rRNA microbiome sequencing was conducted at Novogene Co., Ltd. Total DNA was extracted using a fecal genomic DNA kit (TianGen, Beijing). 16S rRNA libraries (V3–V4 regions) were generated from the extracted DNA, and the libraries were sequenced on the Illumina NovaSeq platform to synthesize the raw

data, and then analyzed for the diversity and abundance of microbial communities in the samples.

2.13 Determination of SCFA

The sample (20 mg) ground in liquid nitrogen was weighed, mixed with 80% methanol solution, and centrifuged at 12,000 rpm and 4 °C for 10 min. Subsequently, 50 μL of the supernatant was derivatized with 150 μL of derivatization reagent at 40 °C for 40 min, diluted 100-fold with 80% methanol solution, and finally analyzed by liquid chromatography-mass spectrometry (LC-MS).

2.14 Untargeted metabolomics

Metabolomic sequencing and analysis were conducted by Novogene Co., Ltd. (Beijing, China). Fecal metabolites from mice were extracted and analyzed using liquid chromatography-tandem mass spectrometry (LC-MS/MS). The raw data were processed with Compound Discoverer 3.3 (ThermoFisher) for spectral analysis and database searching to enable both qualitative and quantitative identification of metabolites. Subsequent statistical analyses were performed using R (v3.4.3), Python (v2.7.6), and CentOS (v6.6).

2.15 Statistical analysis

Data were analyzed using GraphPad Prism and were presented as mean ± standard deviation (SD). Group comparisons were conducted using Student's *t*-test or one-way analysis of variance (ANOVA). Statistical significance was set at ns, $^{*}P < 0.05$, and $^{**}P < 0.01$; ns denotes not statistically significant.

3 Results and discussion

3.1 Synthesis and characterization of Mn_2(Olsa) MOF and Mn_2(Olsa)/Gel

Capitalizing on Olsalazine's (Olsa) established clinical efficacy in IBD management and its structural versatility (notably the capacity to coordinate transition metals into nanoscale MOFs) [10], we pioneered the de novo synthesis of rod-shaped Mn_2(Olsa) MOF particles via hydrothermal method (Fig. 1(a)). The synthesis parameters for Mn_2(Olsa) were systematically screened by varying Mn/Olsa molar ratios, reaction times, and temperatures (Figs. S1 and S2 in the ESM), and the results showed that at a Mn/Olsa molar ratio of 2:1 (Fig. S2(a) in the ESM), a reaction time of 12 h (Fig. S2(b) in the ESM) and a reaction temperature of 80 °C (Fig. S2(c) in the ESM), the yield of Olsa production could reach about 95%, and the PXRD results showed that these MOFs were isostructural (similar diffraction peaks) (Fig. 1(b)). To verify the synthesis and composition of Mn_2(Olsa), elemental mapping analysis was performed (Fig. 1(c)), which showed that C, Mn, N and O elements were uniformly distributed in the Mn_2(Olsa), and morphologically, it was a rod-like structure with a width of about 0.1 μm and a length of 0.6–0.9 μm (Fig. 1(d)). XPS provided a more detailed chemical composition of Mn_2(Olsa), identifying the presence of C, Mn, N and O elements (Fig. 1(e)). In the Mn 2p spectrum in Fig. 1(f), the 641.7 and 653.48 eV peaks of Mn 2p belong to Mn $2p_{3/2}$ and Mn $2p_{1/2}$, respectively, indicating that Mn^{2+} exist mainly in Mn species [23]. The content of manganese in Mn_2(Olsa) was finally determined to be 7.15%, and it was measured using ICP-OES.

To further improve the colon retention of Mn_2(Olsa), a composite hydrogel based on YG and KGM was further prepared for the treatment of IBD through the formation of Olsa-based MOF/composite gels (Fig. 1(h)). SEM imaging revealed a well-defined porous structure in the Mn_2(Olsa)/Gel composite, with homogeneously embedded rod-shaped Mn_2(Olsa) MOF particles distinctly resolved within the matrix (Figs. 1(i) and 1(j)). A critical barrier in oral IBD therapy lies in ensuring site-specific drug release while circumventing gastric degradation. To evaluate the pH-responsive release profile of Mn_2(Olsa)/Gel, we employed physiologically relevant pH gradients simulating gastrointestinal transit, with Olsa and Gel serving as controls. Olsa showed a sustained and rapid release from the simulated intestinal fluid, with a release rate of 69.90% at 4 h, whereas the release rates from the Mn_2(Olsa) and Mn_2(Olsa)/Gel were 41.10% and 27.67%, respectively, which was attributed to the presence of the MOF structure, it played an important role in achieving sustained release of the drug. In the simulated colonic environment with a pH of 7.8, Mn_2(Olsa) and Mn_2(Olsa)/Gel achieved accelerated release as the solubility of Olsa increased (Fig. 1(g)), the controlled release profile of Mn_2(Olsa)/Gel facilitated precision drug delivery to IBD lesions. *In vivo*, FITC-labeled Mn_2(Olsa)/Gel exhibited prolonged fluorescence signals detectable up to 24 h post-administration, confirming the strong intestinal adhesiveness and retention capacity of Mn_2(Olsa)/Gel (Figs. 1(k) and 1(l)), consistent with *in vitro* release profiles. Rheological profiling of Gel and Mn_2(Olsa)/Gel at variable strains, times, and angular frequencies (Figs. 1(m)–1(o)) showed the energy storage modulus (G') > the loss modulus (G") for both systems, verifying hydrogel formation. The significantly elevated G" of Mn_2(Olsa)/Gel relative to Gel further suggested superior viscous behavior, correlating with extended gastrointestinal retention capacity. Overall, we developed an eco-friendly synthesis of rod-shaped Mn_2(Olsa) MOF particles and pioneered the prebiotic-based Mn_2(Olsa)/Gel composite using YG@KGM hydrogel. This innovative system ensured intestinal-targeted Olsa release.

3.2 Anti-oxidative stress and anti-inflammatory effects of Mn_2(Olsa) *in vitro*

Biocompatibility, anti-oxidative stress and anti-inflammatory effects of Mn_2(Olsa) were evaluated using Raw264.7 macrophages and CT26 cells. Raw264.7 cells at a concentration of 150 μg/mL (Fig. 2(a)) and CT26 cells at a concentration of 200 μg/mL (Fig. 2(d)) treated with Mn_2(Olsa) for 24 h did not show significant cytotoxic effects, suggesting the excellent cytocompatibility of Mn_2(Olsa). Studies have shown that excessive ROS production damages intestinal mucosal cells, causing protein structural disruption, lipid peroxidation and DNA damage, which in turn disrupts the integrity of the intestinal barrier and ultimately induces and exacerbates intestinal inflammation [24]. H_2O_2-treated Raw264.7 and CT26 cells served as an oxidative stress model for assessing Mn_2(Olsa)'s potent ROS-scavenging capacity. The CCK8 assay showed that Raw264.7 cell viability was 41.74% after stimulation with 5 mM H_2O_2 (Fig. 2(b)), whereas 125 μg/mL Mn_2(Olsa) restored viability to 90% (Fig. 2(c)). In CT26 cells, 5 mM H_2O_2 reduced viability to 55.92% (Fig. 2(e)), while 50 μg/mL Mn_2(Olsa) restored it to more than 95% (Fig. 2(f)). Flow cytometry analysis confirmed H_2O_2-induced apoptosis (Fig. 2(g)), which was significantly attenuated by Mn_2(Olsa) in a concentration-dependent manner (Fig. S4 in the ESM). Furthermore, Mn_2(Olsa) treatment effectively normalized intracellular ROS levels in H_2O_2-stimulated macrophages (Fig. 2(h)). To visually assess Mn_2(Olsa)'s anti-

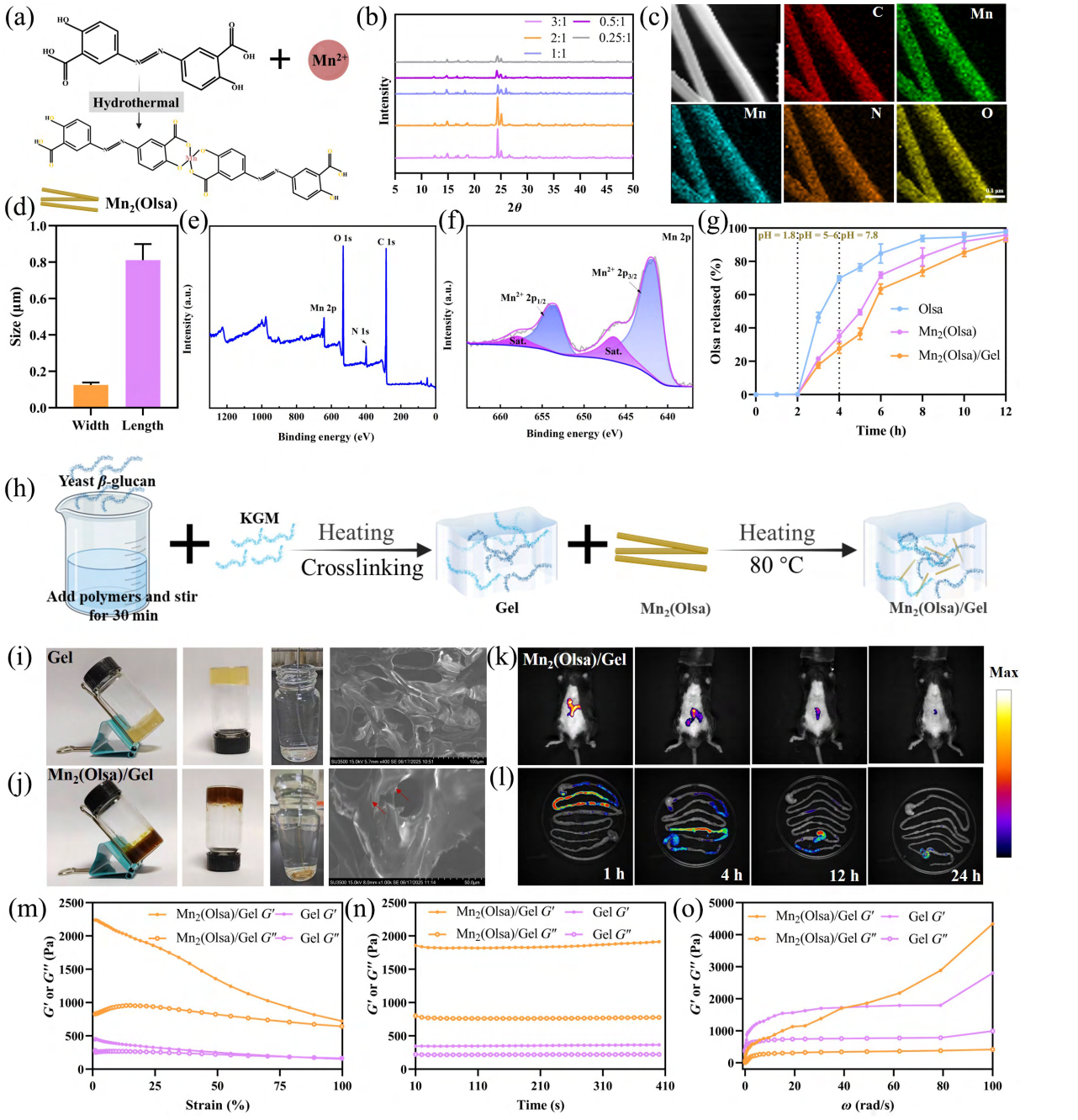


Figure 1 Physicochemical characterization of Mn_2(Olsa) and Mn_2(Olsa)/Gel. (a) Schematic illustration of Mn_2(Olsa) synthesis. (b) PXRD of Mn_2(Olsa). (c) TEM image and corresponded elemental mapping of Mn_2(Olsa). Scale bar: 0.1 μm. (d) The length and width of Mn_2(Olsa). (e) Full-range XPS curve and (f) Mn 2p spectrum. (g) *In vitro* drug release behavior of Olsa, Mn_2(Olsa) and Mn_2(Olsa)/Gel under simulated gastrointestinal environmental conditions (n = 3). (h) Schematic illustration of Mn_2(Olsa)/Gel formation. Photographs and SEM images of (i) Gel and (j) Mn_2(Olsa)/Gel. (k) Representative IVIS images of mice after Mn_2(Olsa)/Gel treatment (n = 3). (l) Representative IVIS images of gastrointestinal tracts after Mn_2(Olsa)/Gel treatment (n = 3). (m) Modulus–strain, (n) time, and (o) angular frequency curves of Gel and Mn_2(Olsa)/Gel.

oxidative efficacy, Calcein-AM/PI double-staining characterized 5 mM H_2O_2-induced damage in Raw264.7 macrophages. As shown in Fig. 2(i), there were a large number of red-marked dead cells in the H_2O_2-treated group. Interestingly, the intensity of red fluorescence was reduced after Mn_2(Olsa) treatment, confirming that Mn_2(Olsa) was effectively able to scavenge ROS and thus protect cells from oxidative damage. Mitochondrial dysfunction induced early apoptosis, JC-1 staining reflected mitochondrial membrane potential (MMP), H_2O_2 induction triggered a decrease in MMP as evidenced by an increase in green monomers (Fig. 2(j)), whereas Mn_2(Olsa) intervention increased MMP as evidenced by an increase in red fluorescent aggregates and restoration of the proportion of J-aggregates/J-monomer fluorescence intensity, which effectively attenuated the H_2O_2-induced oxidative damage and improved mitochondrial dysfunction induced by massive ROS. We simultaneously determined the scavenging capacity of Mn_2(Olsa) for ABTS and DPPH free radicals, where DPPH strategy could be used to assess the total free radical scavenging ability of

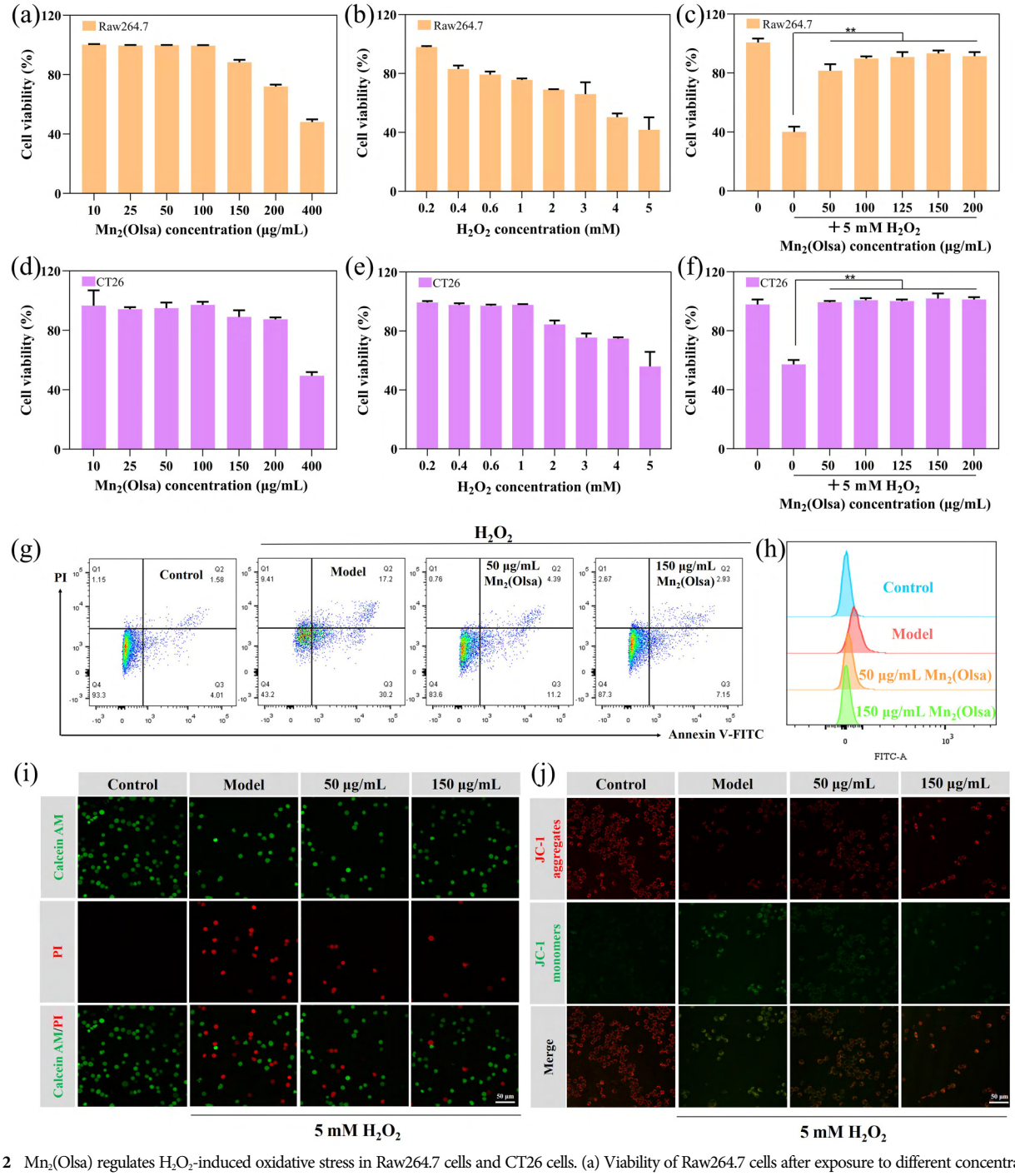


Figure 2 $Mn_2(Olsa)$ regulates H_2O_2-induced oxidative stress in Raw264.7 cells and CT26 cells. (a) Viability of Raw264.7 cells after exposure to different concentrations of $Mn_2(Olsa)$ and (b) H_2O_2 using the CCK-8 method (n = 3). (c) The protective effect of different concentrations of $Mn_2(Olsa)$ intervention on Raw264.7 cells treated with H_2O_2 (n = 3). Viability of CT26 cells after exposure to (d) different concentrations of $Mn_2(Olsa)$ and (e) H_2O_2 using the CCK-8 method (n = 3). (f) The protective effect of different concentrations of $Mn_2(Olsa)$ intervention on CT26 cells treated with H_2O_2 (n = 3). (g) Flow cytometry analysis of the percentage of apoptotic cells in Annexin V-FITC/PI stained Raw264.7 cells after different treatments. (h) The ROS levels in RAW264.7 cells induced by H_2O_2 after different $Mn_2(Olsa)$ treatments were detected by flow cytometry. (i) Calcein-AM/PI fluorescence images of Raw264.7 cells after $Mn_2(Olsa)$ intervention with H_2O_2 stimulation. Scale bar: 50 μm. (j) CLSM images of mitochondrial membrane potential in Raw264.7 cells after $Mn_2(Olsa)$ intervention with H_2O_2 stimulation. Scale bar: 50 μm.

$Mn_2(Olsa)$ and ABTS was used to assess the ability to counteract free radical oxidation [25]. The results showed that $Mn_2(Olsa)$ at a concentration of 32 μg/mL were able to scavenge more than 85% of ABTS radicals, while $Mn_2(Olsa)$ at a concentration of 50 μg/mL were able to neutralize more than 75% of DPPH radicals (Fig. S5 in the ESM). These results confirm $Mn_2(Olsa)$ as a potent ROS scavenger capable of normalizing ROS levels in the inflamed colon.

Macrophages, the predominant infiltrating immune cells within IBD inflamed tissues, can internalize particles ranging from 250 nm to 3 μm via phagocytosis and macropinocytosis [26]. Bio-TEM analysis confirmed macrophage uptake of $Mn_2(Olsa)$ (Fig. 3(a)). To assess its anti-inflammatory activity, we established an *in vitro*

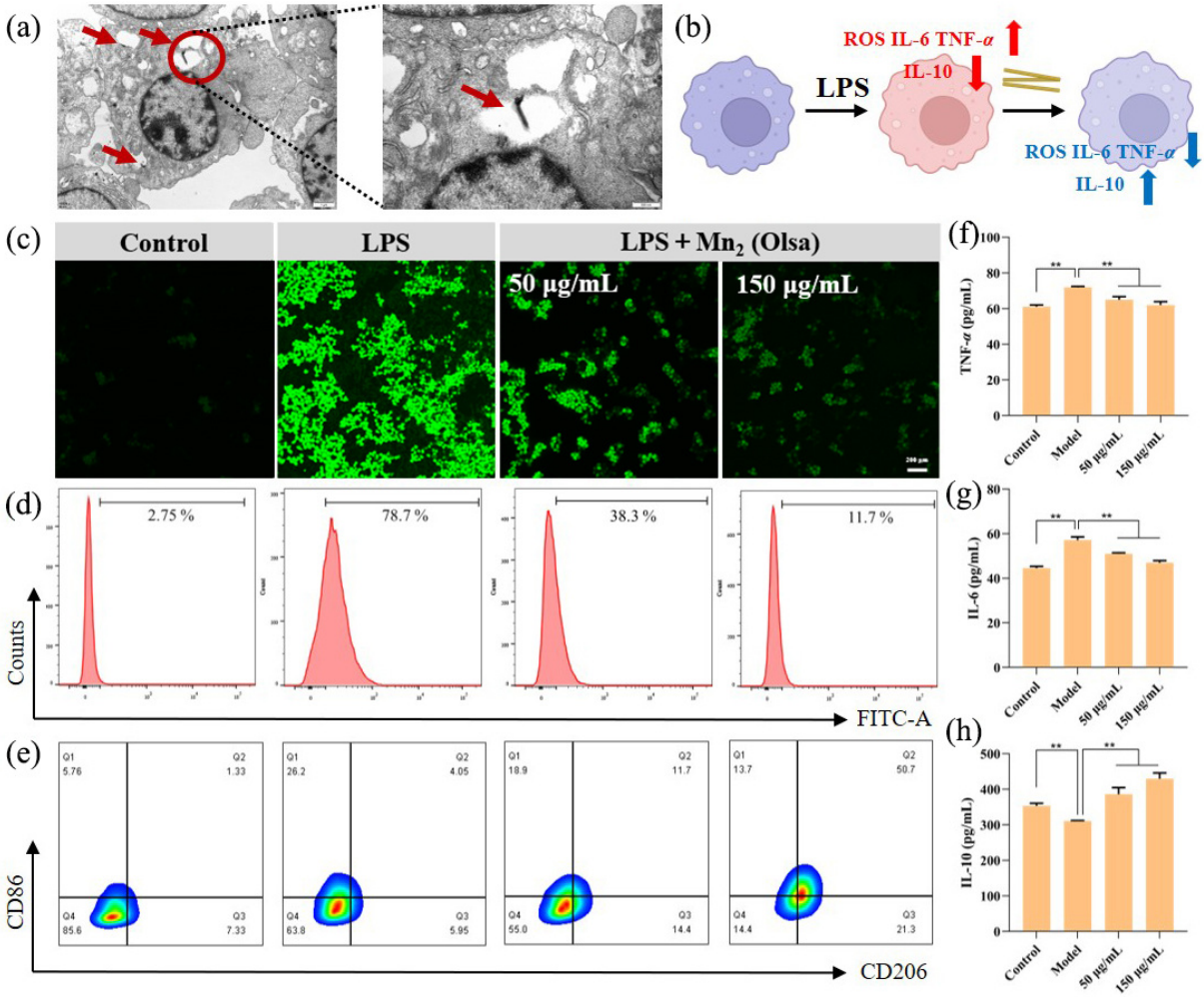


Figure 3 Mn_2(Olsa) regulates LPS-induced macrophage inflammation. (a) Bio-TEM images of RAW264.7 cells treated with Mn_2(Olsa) for 24 h. (b) Schematic diagram of experimental changes in LPS-treated RAW264.7 cells. (c) Fluorescent images and (d) flow cytometry results of intracellular ROS levels after different Mn_2(Olsa) treatments (n = 3). Scale bar: 200 μm. (e) Flow cytometry analysis of the proportion of $CD86^+$ and $CD206^+$ macrophages (n = 3). The levels of pro-inflammatory cytokines (f) TNF-α, (g) IL-6, and (h) anti-inflammatory cytokine IL-10 were detected by ELISA (n = 3).

inflammation model using LPS-stimulated Raw264.7 cells (Fig. 3(b)). As shown in Fig. 3(c), LPS induced an excessive immune response in macrophages, contributing to the production of large amounts of ROS. The CLSM results showed an increase in the intensity of green fluorescence, which was significantly weakened by Mn_2(Olsa) treatment, and the flow cytometry results also demonstrated a decrease in the intensity of fluorescence by Mn_2(Olsa) treatment (Fig. 3(d)). Under IBD conditions, pro-inflammatory M1-type macrophages extensively infiltrate the intestinal mucosa, and their secretion of pro-inflammatory cytokines exacerbates disruption of the intestinal microenvironment [22]. Furthermore, elevated ROS levels can promote macrophage polarization toward the pro-inflammatory phenotype [27]. Therefore, shifting macrophages from the M1 to the anti-inflammatory M2 phenotype represents a promising therapeutic strategy for IBD. We further evaluated the capacity of Mn_2(Olsa) to modulate macrophage phenotype switching by detecting surface markers specific to M1 (CD86) and M2 (CD206) macrophages. Flow cytometry was employed to quantify the proportions of $CD86^+$ and $CD206^+$ cells (Fig. 3(e)). Compared to LPS stimulation alone, Mn_2(Olsa) treatment significantly reduced the proportion of $CD86^+$ macrophages from 26.2% to 13.7%, while markedly increasing the proportion of $CD206^+$ macrophages from 5.95% to 21.3% (Fig. S3 in the ESM). These results demonstrate that Mn_2(Olsa) effectively suppressed the pro-inflammatory M1 phenotype and promoted macrophage polarization toward the anti-inflammatory M2 phenotype, thereby enhancing anti-inflammatory capacity. This phenotypic shift was further corroborated at the cytokine level: LPS stimulation substantially elevated pro-inflammatory cytokines (TNF-α, IL-6) while suppressing the anti-inflammatory cytokine IL-10. Mn_2(Olsa) treatment effectively reversed these effects (Figs. 3(f)–3(h)).

3.3 Treatment of DSS-induced acute colitis mouse model

The *in vivo* efficacy of Mn_2(Olsa)/Gel was further evaluated by constructing a model of DSS-induced IBD, which is schematically shown in Fig. 4(a). Acute colitis is typically characterized by weight loss, increased DAI, and colon shortening. At the experimental endpoint, the therapeutic effect of Mn_2(Olsa)/Gel was visually assessed based on perianal conditions in each mouse group. Mn_2(dobp)/Gel was used as a control. Dobp is structurally similar to Olsa but lacks an azo group and exhibits no reported bioactivity. Since Mn_2(dobp) and Mn_2(Olsa) have similar ligand structures,

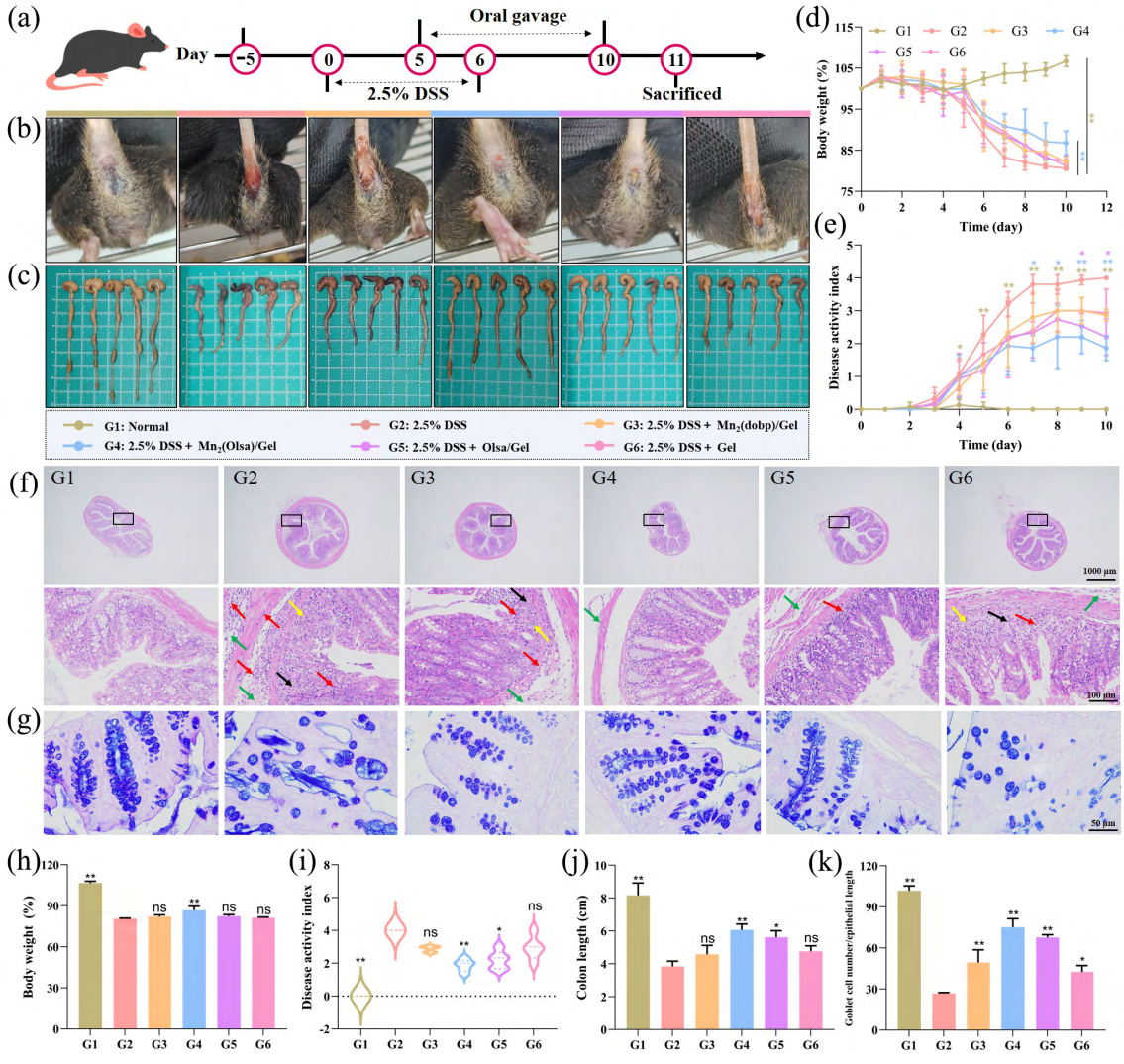


Figure 4 Therapeutic efficacy of Mn_2(Olsa)/Gel in the mouse model of DSS-induced acute colitis. (a) The timeline of acute colitis mouse model construction and drug administration. (b) Representative images showing rectal bleeding and wet tail in mice from different treatment groups. (c) Photographs of the colon of different groups of mice. (d) Daily body weight change and (e) disease activity index of mice from various groups (n = 5). (f) Representative H&E staining images of the colon tissues from different groups at low magnification (top, scale bar: 1000 μm) and high magnification (bottom, scale bar: 100 μm) (n = 3). (g) AB-PAS staining images of the colon tissues from different groups (n = 3). Scale bar: 50 μm. (h) Body weights of the mice in different groups on day 10 and (i) the disease activity index of the mice in different groups on day 10 (n = 5). (j) Quantification of colon length (n = 5). (k) Quantification of the number of goblet cells (n = 3). Data are presented as mean ± SD. Statistical analysis was performed by one-way ANOVA. *P < 0.05, **P < 0.01, compared with the DSS-induced group; ns indicates not statistically significant.

their crystal structures are also highly similar (Fig. S6 in the ESM). Compared to normal mice, DSS-induced mice exhibited severe diarrhea and bloody stools (Fig. 4(b)). All drug treatments ameliorated these colitis symptoms to varying degrees. As a critical marker of intestinal injury severity [28], colon length was significantly restored by oral Mn_2(Olsa)/Gel administration over 5 days (Fig. 4(c)). Compared to the DSS-induced group, colon length increased by 57.81% in the Mn_2(Olsa)/Gel group, 19.27% in the Mn_2(dobp)/Gel group, 46.35% in the Olsa/Gel group and 23.96% in the Gel group (Fig. 4(j)), respectively. The body weights of the mice in each group were also recorded continuously (Fig. 4(d)). As shown in Fig. 4(h), mice in the 2.5% DSS-induced group showed a significant weight loss, whereas oral administration of Mn_2(Olsa)/Gel significantly attenuated the weight loss (P < 0.01). The therapeutic efficacy of Mn_2(Olsa)/Gel against acute colitis was further evaluated through longitudinal monitoring of DAI, calculated from body weight loss, stool consistency and blood. DSS-induced mice exhibited progressively elevated DAI scores versus normal controls over time (Fig. 4(e)). Mn_2(Olsa)/Gel treatment significantly attenuated this increase (P < 0.01), achieving near-normalization by day 10 (Fig. 4(i)).

In addition, histological analysis of colon specimens was performed using H&E staining. As shown in Fig. 4(f), the DSS-induced group exhibited multiple ulcers (black arrow), severe crypt destruction (yellow arrow), edema (green arrows), and substantial inflammatory cell infiltration (red arrow). Treatment with Mn_2(Olsa)/Gel markedly attenuated these histopathological alterations and resulted in a lower histological score compared to the other treatment groups (Fig. S7 in the ESM) (P < 0.01). Goblet cells produce mucin, an important component of the intestinal mucus layer, to prevent the invasion of pathogens and harmful substances [29]. AB-PAS results showed that abundant goblet cells were present in all treatment groups and the number of goblet cells was significantly higher than that of the DSS-induced group

(Figs. 4(g) and 4(k)). These findings suggest early intervention with Mn_2(Olsa)/Gel may curb progression to severe colitis.

3.4 Effect of Mn_2(Olsa)/Gel on the restoration of the intestinal microenvironment

Intestinal barrier function relies fundamentally on epithelial tight junction (TJ) integrity, wherein TJ damage induces pathological increases in intestinal permeability [30]. Early-stage IBD is characterized by increased intestinal mucosal barrier permeability [31], which correlates with altered expression of tight junction proteins (ZO-1, Claudin-1) [32]. Immunofluorescence staining revealed significant downregulation of ZO-1 and Claudin-1 in DSS-induced mice (Figs. 5(a)–5(c)), demonstrating TJ disruption and intestinal barrier compromise. Therapeutic interventions restored TJ integrity, with Mn_2(Olsa)/Gel groups showing marked upregulation of both proteins versus model controls ($P < 0.05$). This correlated with functional recovery of intestinal barrier properties. Meanwhile, we further evaluated the anti-inflammatory activity of Mn_2(Olsa)/Gel *in vivo*. As expected, Mn_2(Olsa)/Gel was able to significantly reduce the levels of pro-inflammatory factors (TNF-α and IL-6) and increase the levels of anti-inflammatory factor (IL-10) ($P < 0.01$), and the effect was close to that of the normal group (Figs. 5(d)–5(f)). Macrophages exhibit functional plasticity, differentiating into M1 (pro-inflammatory) or M2 (anti-inflammatory) types that regulate cytokine secretion and maintain mucosal homeostasis [33]. IBD pathogenesis involves M1/M2 polarization imbalance [34], characterized clinically by elevated M1-type macrophage prevalence and impaired M2-type polarization in patients [35]. Representative immunofluorescence images and semiquantitative analysis intuitively showed that Mn_2(Olsa)/Gel decreased iNOS (M1-marker) expression while increasing Arg-1 (M2-marker) expression, which was consistent with the cytokine

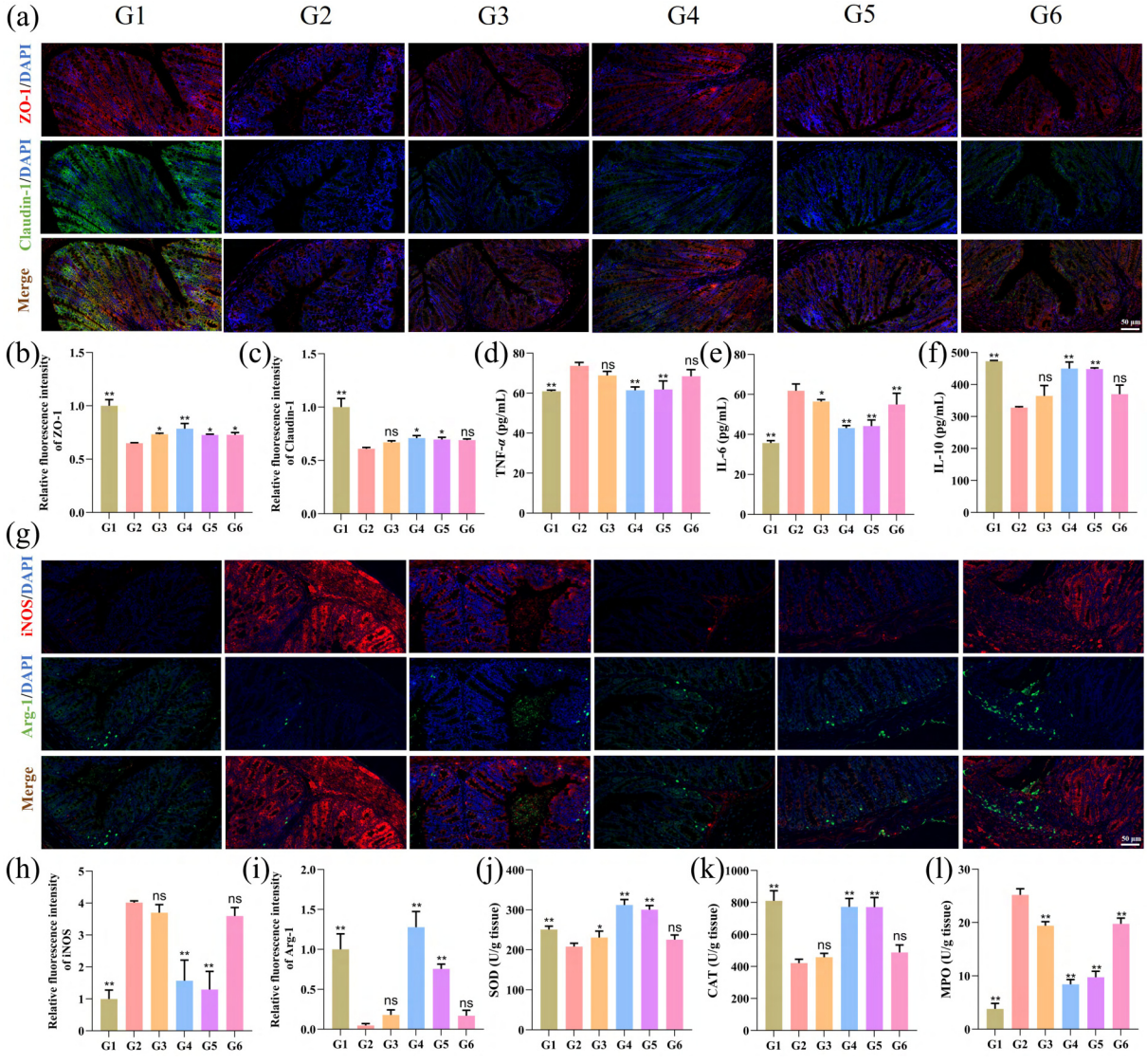


Figure 5 Effects of Mn_2(Olsa)/Gel on the intestinal microenvironment. (a) Representative immunofluorescence images of ZO-1 (red) and Claudin-1 (green) in colon tissues ($n = 3$). Scale bar: 50 μm. Semiquantitative analysis of (b) ZO-1 and (c) Claudin-1 in the colon tissues ($n = 3$). Colonic levels of pro-inflammatory cytokines (d) TNF-α and (e) IL-6 and (f) anti-inflammatory IL-10 ($n = 5$). (g) Representative immunofluorescence images of M1-like macrophage marker iNOS (red) and M2-like macrophage marker Arg-1 (green) in colon tissues ($n = 3$). Scale bar: 50 μm. Semiquantitative analysis of (h) iNOS and (i) Arg-1 in the colon tissues ($n = 3$). The activities of (j) SOD and (k) CAT and (l) the level of MPO in colonic tissues ($n = 5$). Data are presented as mean ± SD. Statistical analysis was performed by one-way ANOVA. $^*P < 0.05$, $^{**}P < 0.01$, compared with the DSS-induced group; ns indicates not statistically significant.

measurements described above, suggesting that Mn_2(Olsa)/Gel alleviated IBD M1/M2 polarization imbalance, repaired the intestinal immune homeostasis, reduced intestinal wall inflammation, and promoted intestinal mucosal repair (Figs. 5(g)–5(i)). In addition, the modulatory effect of Mn_2(Olsa)/Gel on oxidative stress in IBD mice *in vivo* was further demonstrated, mainly in terms of its significant enhancement of SOD, CAT and MPO activities (Figs. 5(j)–5(l)). Taken together, our results suggest that Mn_2(Olsa)/Gel could delay the progression of IBD by restoring the integrity of the colonic epithelial barrier, modulating intestinal immunity, and decreasing the levels of intestinal inflammation and oxidative stress. Although precise quantitative contributions remain to be determined, the three components operate in a coordinated, mutually reinforcing cascade: Mn^{2+}-mediated ROS elimination creates a favorable microenvironment that sensitizes the inflamed tissue to olsalazine, enhancing its anti-inflammatory efficacy; concurrently, the reduced inflammatory burden and modulated redox status collectively shape a beneficial shift in the gut microbiota, which in turn reinforces intestinal homeostasis. This interdependent cascade, rather than any single isolated function, constitutes the core rationale of our multimodal strategy.

3.5 Treatment of DSS-induced chronic colitis mouse model

The therapeutic effect of Mn_2(Olsa)/Gel was further confirmed in a chronic colitis mouse model. Compared to other treatments, Mn_2(Olsa)/Gel significantly ameliorated disease symptoms, most notably by alleviating weight change (about 98% improvement), reducing the DAI (to 0.053), and restoring colon length (to 7.32 cm) (Figs. 6(a)–6(i)). H&E staining evaluation revealed that colon tissue structure was significantly more intact in the Mn_2(Olsa)/Gel-treated group compared to other groups (Fig. S8 in the ESM). Pathological alterations, including severe crypt destruction (yellow arrow), ulcers (black arrow), inflammatory cell infiltration (red arrow), and edema (green arrows), were markedly reduced. The tissue morphology in the Mn_2(Olsa)/Gel group closely resembled that of healthy mice (Fig. 6(d)). Consistent with these findings, ELISA revealed significantly reduced TNF-α and IL-6 levels alongside elevated IL-10 expression in intestinal tissues of Mn_2(Olsa)/Gel-treated mice (Figs. 6(j)–6(l)). These results confirm Mn_2(Olsa)/Gel's efficacy in chronic colitis treatment. In addition, H&E staining revealed that oral administration of Mn_2(Olsa)/Gel induced no damage to the major organs (heart, liver, spleen, lungs, and kidneys) (Fig. S9(a) in the ESM). Furthermore, all detected indicators remained unaffected by Mn_2(Olsa)/Gel treatment (Fig. S9(b) in the ESM), collectively demonstrating its good biocompatibility.

3.6 Behavioral changes in the DSS-induced colitis mouse model

Given the high prevalence of psychological comorbidities in IBD—affecting approximately 30% and 25% of patients for anxiety and depressive symptoms, respectively [36], we evaluated the therapeutic potential of Mn_2(Olsa)/Gel for IBD-associated anxiety and depression. This investigation was motivated by both its established efficacy in IBD treatment and the documented neuroprotective effects of YG against cognitive impairment [15, 16]. In the open field test, IBD model mice exhibited pronounced thigmotaxis (wall-hugging behavior) with minimal center exploration. In contrast, Mn_2(Olsa)/Gel-treated mice displayed significantly increased center dwell time and exploratory trajectories (Fig. S10(a) in the ESM). Total movement distance was markedly elevated in the Mn_2(Olsa)/Gel group (15.47 ± 2.85 m) compared to the model group (7.79 ± 1.28 m, $P < 0.01$), approaching levels observed in healthy controls (18.24 ± 3.67 m) (Figs. 7(a) and 7(b)), indicating improved locomotor function. Elevated plus maze (EPM) testing leverages rodents' innate aversion to open spaces and heights, where reduced open arm time inversely correlates with anxiety-like behavior [37]. Consistent with this principle, DSS-induced model mice spent significantly less time in open arms (2.22 ± 2.69 s, $P < 0.01$) versus healthy controls (115.98 ± 29.23 s) (Figs. 7(c) and 7(d)). Mn_2(Olsa)/Gel treatment substantially increased open arm exploration (62.86 ± 5.73 s, $P < 0.01$ vs. model), with intermediate effects observed in comparator groups: Olsa-treated (24.76 ± 6.45 s), YG-treated (32.94 ± 6.18 s), and Gel-treated (51.52 ± 4.46 s) (Fig. S10(b) in the ESM). For depression-like phenotypes, both tail suspension test (TST, Fig. 7(e)) and forced swimming test (FST, Fig. 7(f)) revealed significantly shortened immobility times in Mn_2(Olsa)/Gel-treated mice relative to DSS controls ($P < 0.01$ for both). Collectively, these behavioral assessments demonstrate the superior efficacy of Mn_2(Olsa)/Gel in mitigating IBD-associated anxiety- and depression-like behaviors.

3.7 Modulation of the gut microbiome *in vivo*

Disturbance of the gut microbiota is a key causative factor in IBD [38]. Characteristically, IBD patients exhibit reduced gut microbiota diversity, diminished populations of beneficial bacteria, and an increased proportion of harmful bacteria. Consequently, therapies targeting the gut microbiota have emerged as an important intervention strategy for IBD treatment [39]. Gut microbiota profiling via 16S rRNA gene sequencing was conducted on DSS-induced mice subjected to various therapies. Analysis of operational taxonomic unit (OTU) distribution (Fig. 8(a), Venn diagram) identified 105 core OTUs common to all groups. Group-specific OTU counts were as follows: normal (514), DSS-induced (232), Olsa-treated (393), YG-treated (487), Mn_2(Olsa)/Gel-treated (736) and Gel-treated (392). Notably, the elevated OTU richness observed in the Mn_2(Olsa)/Gel group relative to the DSS group indicates a potential restoration of microbial diversity by this treatment. Significant differences in α-diversity indices (Shannon, Fig. 8(b); Simpson, Fig. 8(c); Chao1, Fig. 8(d)) were observed between the normal and DSS groups, and between the DSS and treatment groups. These results suggest increased microbial species richness in all treated mice, with the Mn_2(Olsa)/Gel group showing the most pronounced enhancement. Non-metric multidimensional scaling (NMDS) plots of β-diversity also showed significant differences in microbial composition between the normal, DSS and Mn_2(Olsa)/Gel-treated groups (Fig. 8(e)). Composition analyses of the gut microbiota revealed genus-level shifts across groups (Fig. 8(f)). DSS induction markedly enriched *Escherichia-Shigella* (Fig. S11 in the ESM), which was frequently associated with intestinal inflammation in published reports [40–42], consistent with IBD-associated dysbiosis [43]. Concurrent increases in *Klebsiella* [40], *Alistipes* [44] and *Aeromonas* [45] might be involved in intestinal barrier disruption and exacerbated inflammation. Importantly, Mn_2(Olsa)/Gel treatment not only suppressed these potentially harmful taxa but also elevated beneficial genera (*Lachnospiraceae_NK4A136_group*, *Prevotellaceae_UCG-001*, *Ligilactobacillus* and *Alloprevotella*) to levels exceeding those in healthy controls (Fig. 8(g)). Functionally, many members of these

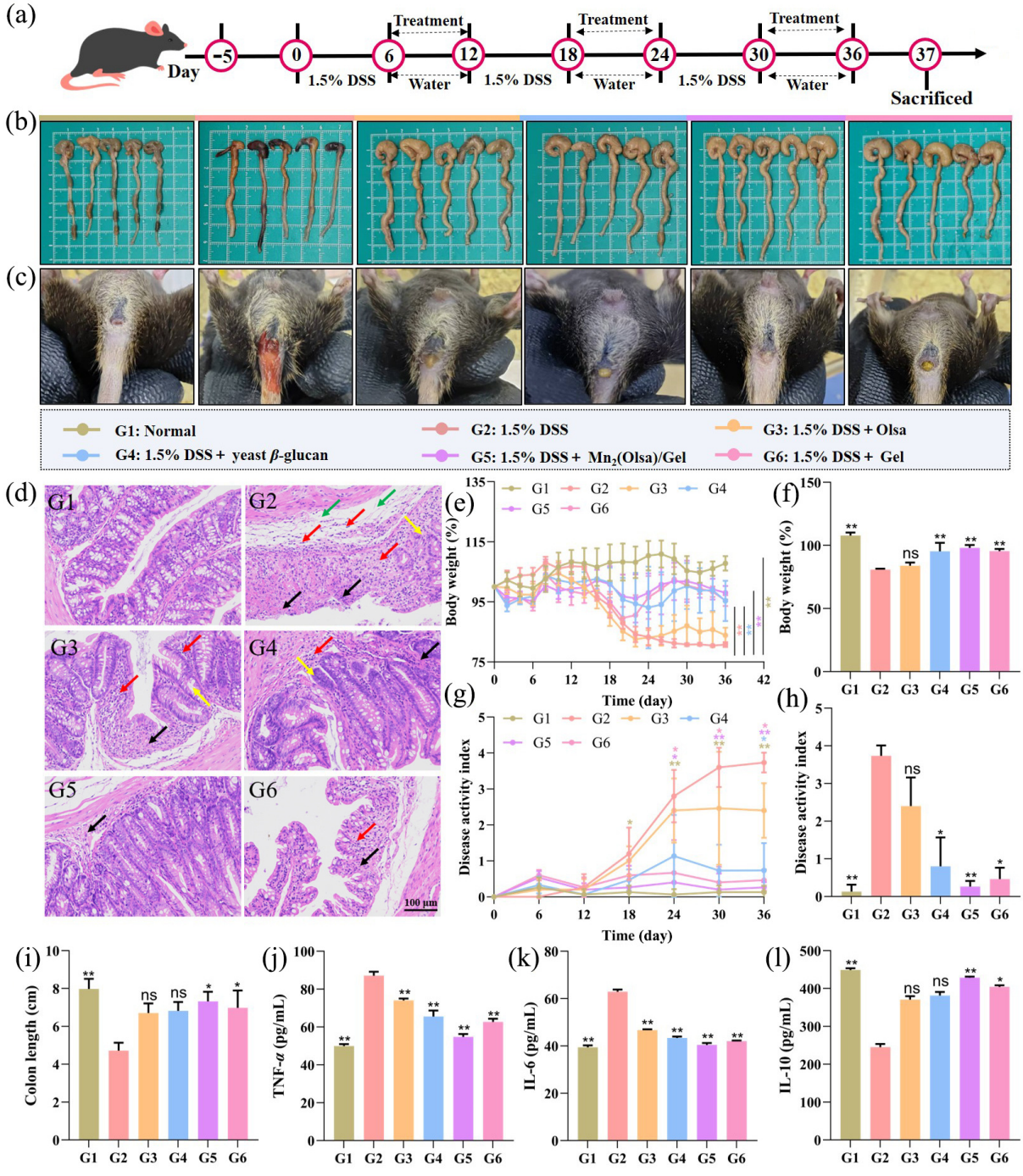


Figure 6 Therapeutic efficacy of Mn_2(Olsa)/Gel in the mouse model of DSS-induced chronic colitis. (a) The timeline of chronic colitis mouse model construction and drug administration. (b) Representative images showing rectal bleeding and wet tail in mice from different treatment groups. (c) Photographs of the colon of different groups of mice. (d) Representative images of H&E-stained tissue sections (n = 3). Scale bar: 100 μm. (e) Changes in body weight of mice in different treatments and (f) body weight of each group on day 36 (n = 5). (g) Changes in DAI score in mice and (h) DAI score of each group on day 36 (n = 5). (i) Length of colon in each group (n = 5). Colonic levels of pro-inflammatory cytokines (j) TNF-α, (k) IL-6 and (l) anti-inflammatory IL-10 (n = 5). Data are presented as mean ± SD. Statistical analysis was performed by one-way ANOVA. *P < 0.05, **P < 0.01, compared with the DSS-induced group; ns indicates not statistically significant.

beneficial genera (*Lachnospiraceae_NK4A136_group* [46, 47], *Prevotellaceae_UCG-001* [48, 49] and *Alloprevotella* [50, 51]) are considered to have the potential for SCFA production. SCFAs have been shown to reinforce mucosal barrier integrity and suppress inflammation [52, 53], thereby potentially mitigating IBD progression. Consistent with this observation, quantitative SCFA analysis revealed a significant decline in acetic acid, propionic acid, butyric acid, valeric acid and isobutyric acid levels (by 49.68%, 46.92%, 92.12%, 53.84%, and 12.65%, respectively) in the DSS group versus the normal group. Conversely, Mn_2(Olsa)/Gel treatment markedly elevated these SCFA levels compared to the DSS group, with increases of 43.55%, 119.22%, 325.99%, 121.40%, and 39.39% for acetic acid, propionic acid, butyric acid, valeric acid and isobutyric acid, respectively (Fig. 8(i)). Similar trends were also

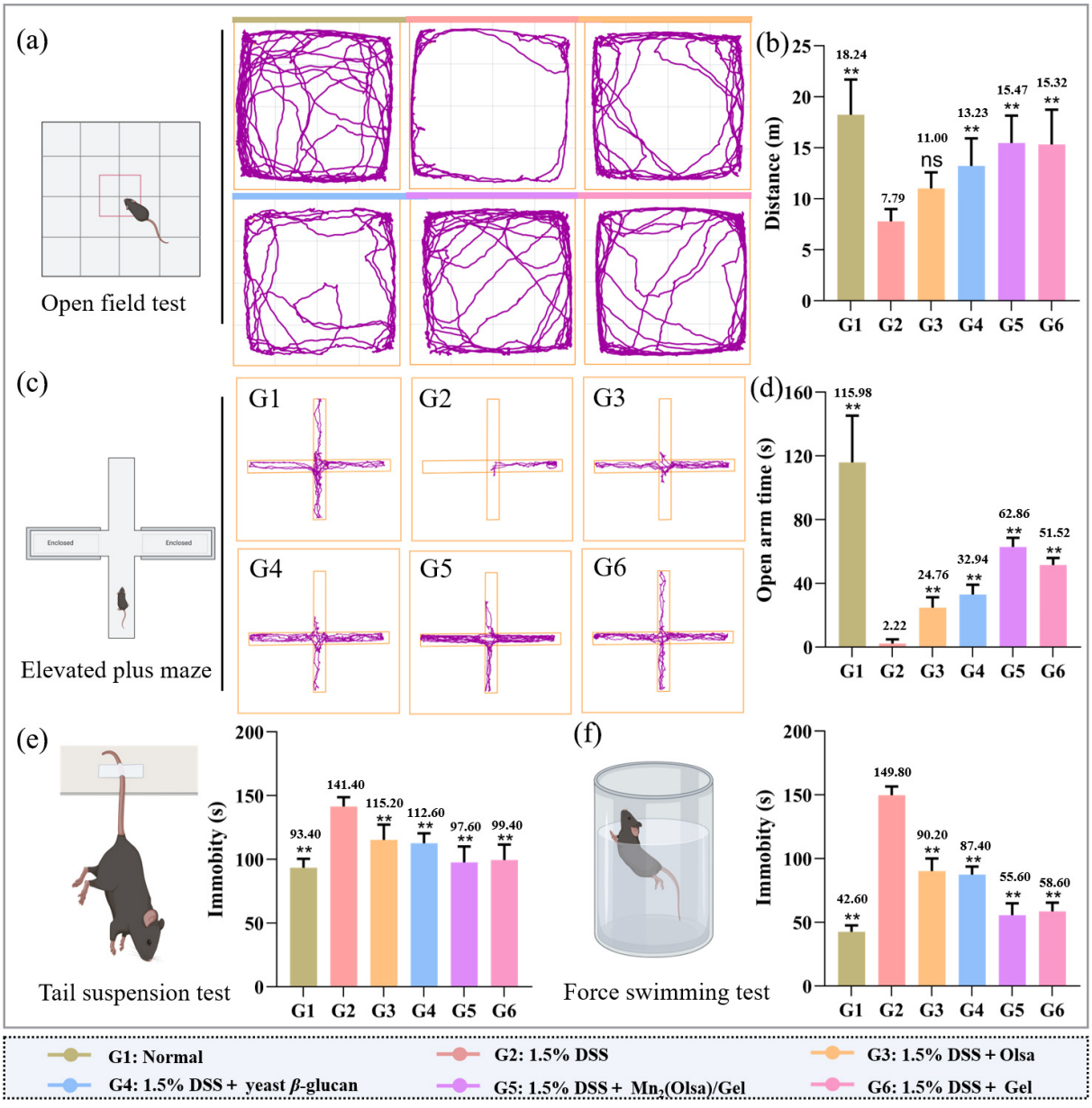


Figure 7 Mn_2(Olsa)/Gel prevents DSS-induced behavioral changes in anxiety and depression associated with colitis in mice. (a) Mouse motion tracking images in the open field test and (b) statistical results of distance traveled ($n = 5$). (c) Mouse motion tracking images in the elevated plus maze and (d) statistical results of open arm time ($n = 5$). (e) Immobility time in the tail suspension test ($n = 5$). (f) Immobility time in the forced swim test ($n = 5$). Data are presented as mean ± SD. Statistical analysis was performed by one-way ANOVA. *$P < 0.05$, **$P < 0.01$, compared with the DSS-induced group; ns indicates not statistically significant.

supported by LEfSe analyses (Fig. 8(h)). Specifically, Mn_2(Olsa)/Gel treatment increased the relative abundance of *Prevotellaceae* (family), *Lachnospiraceae* (family) (both reported to ferment polysaccharides and produce SCFAs) [54–56], *Lachnospirales* (order), and *Oscillospirales* (order) (both associated with SCFA production) [57, 58], and *Clostridia* (class) (shown to contribute to SCFA production) [59]. In contrast, the DSS-induced model group was enriched in *Aeromonadaceae* (family) (usually regarded as an opportunistic pathogen) [60], *Enterobacteriaceae* (family) (positively associated with IBD pathogenesis) [61], *Enterobacterales* (order) (within *Enterobacteriaceae*), and *Gammaproteobacteria* (class) (containing potentially pathogenic members).

3.8 Mechanisms of Mn_2(Olsa)/Gel treatment to alleviate IBD-related anxiety and depression

Given the superior attenuation of IBD-associated anxiety/depressive behaviors by Mn_2(Olsa)/Gel, we investigated its neuroprotective mechanisms. Nissl staining revealed pronounced neuronal loss in hippocampal CA3/DG regions of DSS-induced mice (Fig. 9(a)). Mn_2(Olsa)/Gel treatment preserved neuronal integrity, showing no significant pathology and elevating viable neuron counts to near-normal levels (Figs. S12(a) and S12(b) in the ESM). Immunofluorescence staining of MAP-2, a standard marker for mature neurons, revealed significantly attenuated fluorescence intensity in the hippocampal tissue of DSS-induced mice versus controls (Fig. 9(b)). Mn_2(Olsa)/Gel treatment robustly restored MAP-2 signal and the neuronal connections were more obvious (Fig. S12(c) in the ESM). Immunofluorescence staining characterized neuroinflammation markers: GFAP (astrocyte indicator) and Iba1 (microglia marker). Neuroinflammation or

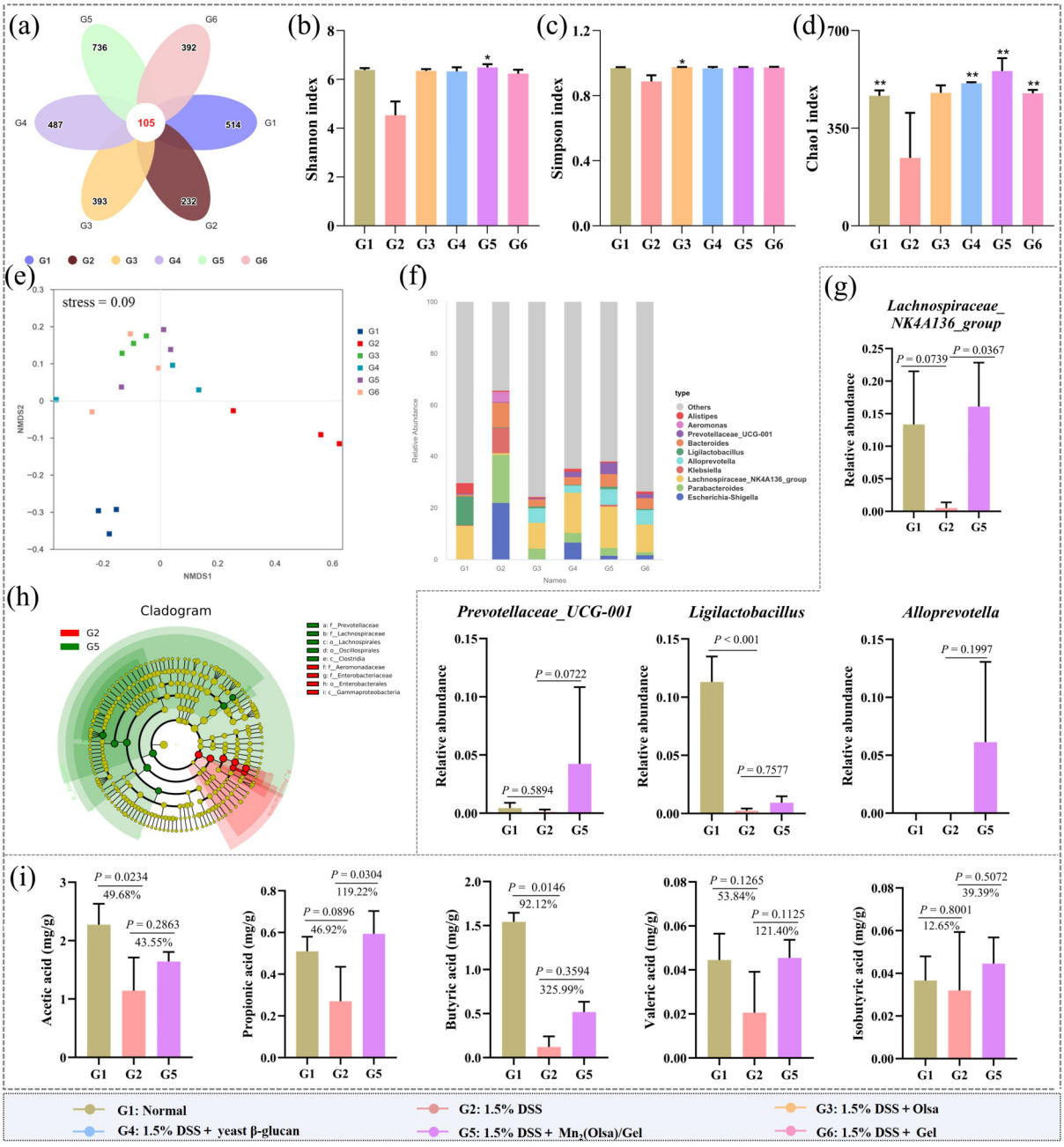


Figure 8 Modulation of gut microbiota in mice with colitis by Mn_2(Olsa)/Gel. (a) Venn diagram of colonic microorganism OTUs. The α-diversity indices of (b) Shannon, (c) Simpson, and (d) Chao1. (e) NMDS score plot of β-diversity of the gut microbiota. (f) Histogram of the relative abundance of the gut microbiome at the genus level. (g) The relative abundance of *Lachnospiraceae_NK4A136_group*, *Prevotellaceae_UCG-001*, *Ligilactobacillus*, and *Alloprevotella*. (h) LEfSe analysis to determine differences in community composition of the gut microbiota between the 1.5% DSS-induced colitis mouse group and the Mn_2(Olsa)/Gel intervention group. (i) The concentration of SCFAs, mainly including acetic acid, propionic acid, butyric acid, valeric acid and isobutyric acid (n = 3). Data are presented as mean ± SD. Statistical analysis was performed by one-way ANOVA. $^*P < 0.05$, $^{**}P < 0.01$, compared with the DSS-induced group.

brain injury triggers GFAP upregulation and astrocyte activation, driving glial scar formation-an adaptive neuroprotective response against neurodegeneration [62]. As shown in Fig. 9(c), there was a trend of elevated GFAP expression in the DSS-induced group, indicating the presence of significant neuroinflammatory injury. In contrast, GFAP expression was significantly down-regulated in the Mn_2(Olsa)/Gel-treated group (Fig. S12(d) in the ESM), indicating some relief of neuroinflammation. In response to inflammatory stimuli in the brain, microglia were activated in response to a significant upregulation of Iba1 expression, which in turn triggered disruption of the blood-brain barrier and exacerbation of neurological damage [63]. Iba1 expression was significantly reduced in hippocampal tissues of Mn_2(Olsa)/Gel-treated IBD mice (Fig. S12(e) in the ESM), suggesting that the treatment was effective in reducing neuroinflammation.

Given the pivotal role of microbial metabolites in gut-brain communication, we conducted a comparative analysis of fecal metabolomic profiles following the various treatments. Multivariate analysis revealed a clear metabolic separation among the groups. Principal component analysis (PCA) and orthogonal partial least

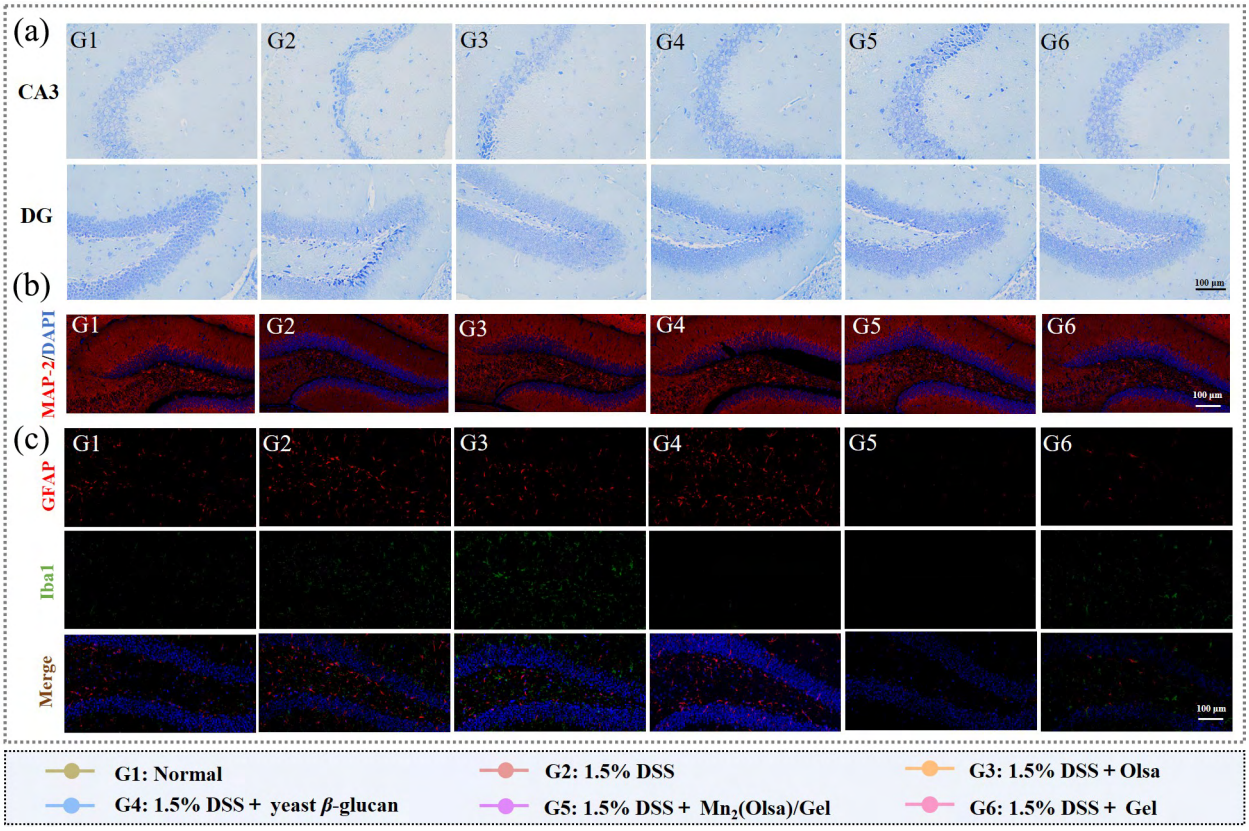


Figure 9 The ameliorative effects of Mn_2(Olsa)/Gel on neurological damage and inflammation in mice with colitis. (a) Nissl staining images of neurons in different groups of the CA3 and DG regions of the hippocampus (n = 3). (b) Immunofluorescence staining images of mature neurons in the hippocampus (MAP-2, red) (n = 3). (c) Immunofluorescence staining images of astrocytes (GFAP, red) and microglia (Iba1, green) in the hippocampus of different groups (n = 3).

squares discriminant analysis (OPLS-DA) score plots demonstrated robust separation between the normal, DSS-induced, and Mn_2(Olsa)/Gel-treated groups, indicating distinct metabolic profiles (Figs. 10(a) and 10(b)). Treatment with Mn_2(Olsa)/Gel significantly reversed the DSS-induced metabolic dysregulation (Fig. 10(c)).

Metabolic profiling via volcano plot analysis demonstrated that Mn_2(Olsa)/Gel treatment significantly reprogrammed the metabolome, altering 198 metabolites (115 upregulated, 83 downregulated) relative to the model group (Fig. S13 in the ESM). This restructuring included the selective regulation of key bioactive metabolites (Fig. 10(d) and Fig. S14 in the ESM), which effectively reversed the DSS-induced accumulation of 3-sulfodeoxycholic acid and enhanced neuroprotective pathways [64]. Specifically, the therapy increased levels of hippuric acid (a GPCR-GPR109A agonist supporting gut-brain axis health) [65], and the neural repair-associated metabolite 2-oxoarginine [66]. The treatment also remodeled glycerophospholipid metabolism [67], marked by upregulated LysoPA(22:5(4Z,7Z,10Z,13Z,16Z)/0:0) and PA(22:5(4Z,7Z,10Z,13Z,16Z)/20:0), alongside downregulated PC(22:5(4Z,7Z,10Z,13Z,16Z)/14:0) and LysoPA(P-16:0/0:0) pertinent to depression pathogenesis [68]. Moreover, Mn_2(Olsa)/Gel significantly boosted levels of SCFAs, such as acetic, propionic, butyric, valeric, and isobutyric acids (Fig. 8(i)). As essential gut-brain mediators, SCFAs mitigate depression and anxiety through multiple mechanisms, including suppression of neuroinflammation, enhancement of intestinal barrier integrity, and modulation of epigenetic and neuroendocrine pathways [69]. The therapeutic effect of Mn_2(Olsa)/Gel against colitis and its neurological comorbidities is mediated by a multi-faceted mechanism. This mechanism entails a synchronized restoration of the gut barrier, resolution of systemic inflammation, and direct neuroprotection, driven by a beneficial reprogramming of key metabolites involving bile acids, glycerophospholipids, neuro-active compounds, and SCFAs. Furthermore, Kyoto Encyclopedia of Genes and Genomes (KEGG) enrichment analysis implicated specific metabolic pathways in these therapeutic effects (Fig. 10(e)), including 2-oxocarboxylic acid metabolism [70], arginine biosynthesis [71], and arginine and proline metabolism [72].

4 Conclusions

In summary, this study developed an oral formulation based on a prebiotic "shield" hydrogel embedded with rod-shaped Mn_2(Olsa) MOF particles (Mn_2(Olsa)/Gel), which ensured sustained intestinal adhesion and retention, facilitating efficient colon-targeted delivery. Further demonstrating its ability to alleviate pathological symptoms and related mental disorders in mice with colitis. Specifically, in DSS-induced acute and chronic colitis mice, Mn_2(Olsa)/Gel reduced intestinal inflammation, lowered oxidative stress levels in the colon, alleviated immune homeostasis imbalance, restored gut microbiota dysbiosis, and improved intestinal barrier damage. Additionally, Mn_2(Olsa)/Gel significantly alleviated mental disorders associated with IBD (such as anxiety- and depression-like behaviors). The underlying mechanisms may involve the regulation of microbiota metabolites, suppression of neuroinflammation, and enhancement of hippocampal neuroplasticity, etc. This work proposes a promising therapeutic strategy for IBD and its psychiatric comorbidities while advancing the design of intestinal-

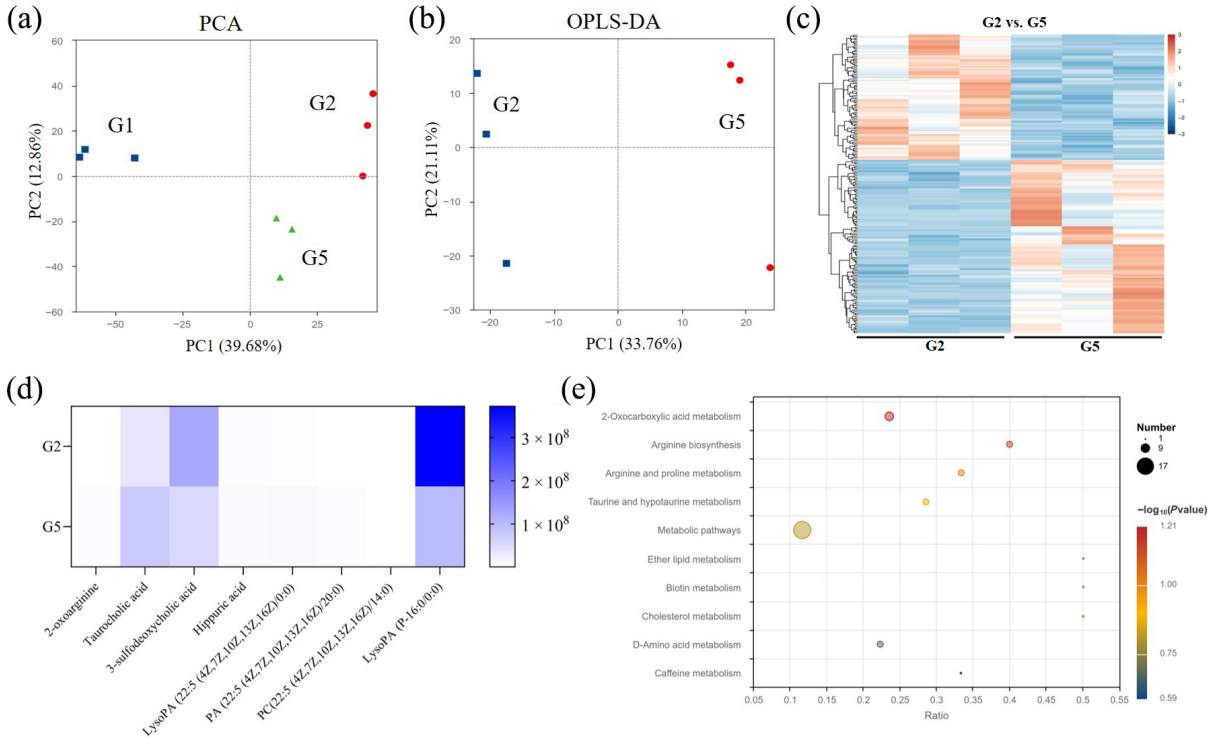


Figure 10 Untargeted metabolomics analysis of fecal samples treated with Mn_2(Olsa)/Gel. (a) PCA and (b) OPLS-DA of the metabolome in the DSS group and Mn_2(Olsa)/Gel-treated group (n = 3). (c) Heatmap illustrating the differential metabolites between the DSS and Mn_2(Olsa)/Gel-treated groups (n = 3). (d) Heatmap of key differential metabolite aggregation in DSS and Mn_2(Olsa)/Gel-treated mice. (e) KEGG enrichment analysis of significantly different metabolites.

microenvironment-targeting polysaccharide-based hydrogels. Notably, the incorporation of Mn^{2+} serves as a functional component in this system. Although no acute toxicity was observed under the current experimental conditions, further investigation is warranted to clarify its long-term biosafety, potential tissue accumulation (particularly in the brain), and possible neurotoxicity. A comprehensive safety evaluation will be essential for enhancing the translational potential of this hydrogel formulation in future clinical applications.

Electronic Supplementary Material: Supplementary material (characterization of Olsa and Mn_2(Olsa), representative images and apoptosis rate of LPS-induced macrophage apoptosis, radical scavenging activity of Mn_2(Olsa), PXRD patterns of Mn_2(Olsa) and Mn_2(dobp), histological scores of the colon in mice with acute and chronic colitis, H&E staining of heart, liver, lung, kidney and spleen, heatmap of mice in the open field test and elevated plus test, the relative abundance of *Escherichia-Shigella*, *Klebsiella*, *Alistipes* and *Aeromonas*, number of live neurons in the CA3 and DG regions, the relative fluorescence intensity of MAP-2, GFAP and Iba1, volcano plot showing differential metabolites, and the relative abundance of key metabolites) is available in the online version of this article at https://doi.org/10.26599/NR.2026.94908754.

Data availability

All data needed to support the conclusions in the paper are presented in the manuscript and/or the Electronic Supplementary Material. Additional data related to this paper may be requested from the corresponding author upon request.

Acknowledgements

This work was supported by the Key project at the central government level: the ability establishment of sustainable use for valuable Chinese medicine resources (No. 2060302) and the National Natural Science Foundation of China (Nos. 82373982 and 82173929).

Declaration of competing interest

The authors declare no conflict of interest.

Author contribution statement

X. Z. W.: Data curation, validation, writing, experimental design, investigation, data analysis. W. Y. S.: Data curation, validation, data analysis. X. L.: Experimental design, investigation, animal experiments resources, supervision, funding acquisition. H. X.: Validation. H. Y. T.: Validation. L. Q. H.: Project administration. L. P. G.: Project administration, funding acquisition. W. Y. G.: Project administration, funding acquisition, supervision.

Informed consent

Not applicable.

Ethics statement

All animal experiments strictly adhered to the Guidelines for Care and Use of Laboratory Animals of the National Institutes of Health and were approved by the Zhongxin Huake (Tianjin) Biotechnology Co., Ltd., number ZXHK-DWLL-2025-0013.

Use of AI statement

None.

References

[1] Neurath, M. F. Host-microbiota interactions in inflammatory bowel disease. *Nat. Rev. Gastroenterol. Hepatol.* **2020**, *17*, 76–77.

[2] Xiong, J. Q.; Fu, Y. F.; Qiu, J. H.; Liao, W. D.; Luo, L. Y.; Chen, S. H. Global research trends of immunotherapy and biotherapy for inflammatory bowel disease: A bibliometric analysis from 2002 to 2021. *BioMed. Eng. OnLine* **2022**, *21*, 42.

[3] Chen, C.; Guilbaud, L.; Marotti, V.; Zhang, W. N.; Domingues, I.; Yagoubi, H.; Vints, K.; Xu, Y. N.; Beloqui, A. An antioxidant metal-organic framework with functional coatings for oral anti-TNF-α antibody delivery in inflammatory bowel disease treatment. *J. Control. Release* **2026**, *389*, 114411.

[4] Song, J. Y.; Wang, T.; Zhang, K. L.; Zhu, P. F.; Yu, Y.; Li, T.; Gong, D. Y.; Zha, L.; Ma, Y. Natural products-integrated drug delivery systems as innovative therapeutic strategies for inflammatory bowel disease management. *Nano Res.* **2025**, *18*, 94908007.

[5] Tu, Z. X.; Zhong, Y. L.; Hu, H. Z.; Shao, D.; Haag, R.; Schirner, M.; Lee, J.; Sullenger, B.; Leong, K. W. Design of therapeutic biomaterials to control inflammation. *Nat. Rev. Mater.* **2022**, *7*, 557–574.

[6] Cui, T. T.; Li, B.; Lou, Z. Y.; Yang, K.; Yan, K. J.; Ding, D. H.; Ge, H. Oral administration of nanozyme-armed probiotic *Escherichia coli* Nissle 1917 with ROS scavenging for inflammatory bowel disease therapy. *Chem. Eng. J.* **2025**, *519*, 164949.

[7] Barberio, B.; Zamani, M.; Black, C. J.; Savarino, E. V.; Ford, A. C. Prevalence of symptoms of anxiety and depression in patients with inflammatory bowel disease: A systematic review and meta-analysis. *Lancet Gastroenterol. Hepatol.* **2021**, *6*, 359–370.

[8] Luo, K. C.; Zhang, M. T.; Tu, Q. W.; Li, J.; Wang, Y. H.; Wan, S. L.; Li, D. J.; Qian, Q.; Xia, L. From gut inflammation to psychiatric comorbidity: Mechanisms and therapies for anxiety and depression in inflammatory bowel disease. *J. Neuroinflamm.* **2025**, *22*, 149.

[9] Ma, T. F.; Gan, G. H.; Cheng, J.; Shen, Z. Q.; Zhang, G. Y.; Liu, S. Y.; Hu, J. M. Engineered probiotics enable targeted gut delivery of dual gasotransmitters for inflammatory bowel disease therapy. *Angew. Chem., Int. Ed.* **2025**, *64*, e202502588.

[10] Zhang, Z. Z.; Pan, Y.; Guo, Z. Y.; Fan, X.; Pan, Q. Q.; Gao, W. X.; Luo, K.; Pu, Y. J.; He, B. An olsalazine nanoneedle-embedded inulin hydrogel reshapes intestinal homeostasis in inflammatory bowel disease. *Bioact. Mater.* **2024**, *33*, 71–84.

[11] Zhang, Y. Z.; He, J.; Zeng, H.; Xu, D. X.; Li, W. L.; Wang, Y. B. Advances in prebiotic carbohydrate-based targeted delivery: Overcoming gastrointestinal challenges for bioactive ingredients. *Food Chem.* **2025**, *466*, 142210.

[12] Jacob, E. M.; Borah, A.; Pillai, S. C.; Kumar, D. S. Inflammatory bowel disease: The emergence of new trends in lifestyle and nanomedicine as the modern tool for pharmacotherapy. *Nanomaterials* **2020**, *10*, 2460.

[13] Yang, F.; Cheung, P. C. K. Fungal β-glucan-based nanotherapeutics: From fabrication to application. *J. Fungi* **2023**, *9*, 2460.

[14] Li, S. C.; Peng, H. H.; Sun, Y. N.; Yang, J. L.; Wang, J.; Bai, F. Q.; Peng, C. Y.; Fang, S. Z.; Cai, H. M.; Chen, G. J. Yeast β-glucan attenuates dextran sulfate sodium-induced colitis: Involvement of gut microbiota and short-chain fatty acids. *Int. J. Biol. Macromol.* **2024**, *280*, 135846.

[15] Lacasa, M.; Alegre-Martin, J.; Sentañes, R. S.; Varela-Sende, L.; Jurek, J.; Castro-Marrero, J. Yeast beta-glucan supplementation with multivitamins attenuates cognitive impairments in individuals with myalgic encephalomyelitis/chronic fatigue syndrome: A randomized, double-blind, placebo-controlled trial. *Nutrients* **2023**, *15*, 4504.

[16] Mo, X. X.; Cheng, R. J.; Shen, L. H.; Liu, N.; Sun, Y. H.; Lin, S.; Jiang, G. H.; Li, X. Q.; Peng, X. B.; Zhang, Y. et al. Yeast β-glucan alleviates high-fat diet-induced Alzheimer's disease-like pathologies in rats via the gut-brain axis. *Int. J. Biol. Macromol.* **2024**, *278*, 134939.

[17] Liu, Z. J.; Ren, X.; Cheng, Y. Q.; Zhao, G. H.; Zhou, Y. Gelation mechanism of alkali induced heat-set konjac glucomannan gel. *Trends Food Sci. Technol.* **2021**, *116*, 244–254.

[18] Yuan, C.; Zou, Y. Y.; Cui, B.; Fang, Y. S.; Lu, L.; Xu, D. Y. Influence of cyclodextrins on the gelation behavior of κ-carrageenan/konjac glucomannan composite gel. *Food Hydrocoll.* **2021**, *120*, 106927.

[19] Geng, X. Y.; Zhao, N.; Song, X. W.; Wu, J. F.; Zhu, Q. M.; Wu, T.; Chen, H. X.; Zhang, M. Fabrication and characterization of konjac glucomannan/oat β-glucan composite hydrogel: Microstructure, physicochemical properties and gelation mechanism studies. *Molecules* **2022**, *27*, 8494.

[20] Ohkuma, S. Use of fluorescein isothiocyanate-dextran to measure proton pumping in lysosomes and related organelles. *Methods Enzymol.* **1989**, *174*, 131–154.

[21] Lai, K.; Pritišanac, I.; Liu, Z. Q.; Liu, H. W.; Gong, L. N.; Li, M. X.; Lu, J. F.; Qi, X.; Xu, T. L.; Forman-Kay, J. et al. Glutamate acts on acid-sensing ion channels to worsen ischaemic brain injury. *Nature* **2024**, *631*, 826–834.

[22] Zhang, X.; Yang, H.; He, Y.; Zhang, D.; Lu, G. F.; Ren, M. D.; Lyu, Y.; Yuan, Z.; He, S. X. Yeast-inspired orally-administered nanocomposite scavenges oxidative stress and restores gut immune homeostasis for inflammatory bowel disease treatment. *ACS Nano* **2025**, *19*, 7350–7369.

[23] Deng, D.; Wang, Y.; Wen, S. H.; Kang, Y. J.; Cui, X. Y.; Tang, R.; Yang, X. P. Metal-organic framework composite Mn/Fe–MOF@Pd with peroxidase-like activities for sensitive colorimetric detection of hydroquinone. *Anal. Chim. Acta* **2023**, *1279*, 341797.

[24] Hu, Q. L.; Li, J. Y.; Wang, T.; Xu, X. C.; Duan, Y. X.; Jin, Y. X. Polyphenolic nanoparticle-modified probiotics for microenvironment remodeling and targeted therapy of inflammatory bowel disease. *ACS Nano* **2024**, *18*, 12917–12932.

[25] Xu, M.; Xin, W.; Xu, J. B.; Wang, A. Y.; Ma, S.; Dai, D.; Wang, Y. D.; Yang, D. M.; Zhao, L.; Li, H. R. Biosilicification-mimicking chiral nanostructures for targeted treatment of inflammatory bowel disease. *Nat. Commun.* **2025**, *16*, 2551.

[26] Manzanares, D.; Ceña, V. Endocytosis: The nanoparticle and submicron nanocompounds gateway into the cell. *Pharmaceutics* **2020**, *12*, 371.

[27] Yang, J. M.; Ye, J. M.; Li, R. T.; Li, R. Y.; Liu, X. T.; Han, J. W.; Yang, Y. W.; Ran, N. N.; Yuan, M. Y.; Zhang, Z. H. et al. Nanozyme-functionalized microalgal biohybrid microrobots in inflammatory bowel disease treatment. *Biomaterials* **2025**, *319*, 123231.

[28] Liang, D. S.; Shen, X. F.; Han, L.; Ren, H.; Zang, T.; Tan, L. L.; Lu, Z. X.; Liao, X. P.; Vetha, B. S. S.; Liu, Y. H. et al. Dual-ROS sensitive moieties conjugate inhibits curcumin oxidative degradation for colitis precise therapy. *Adv. Healthc. Mater.* **2024**, *13*, e2303016.

[29] Yang, S. W.; Yu, M. Role of goblet cells in intestinal barrier and mucosal immunity. *J. Inflamm. Res.* **2021**, *14*, 3171–3183.

[30] Zeisel, M. B.; Dhawan, P.; Baumert, T. F. Tight junction proteins in gastrointestinal and liver disease. *Gut* **2019**, *68*, 547–561.

[31] Vilardi, A.; Przyborski, S.; Mobbs, C.; Rufini, A.; Tufarelli, C. Current understanding of the interplay between extracellular matrix remodelling and gut permeability in health and disease. *Cell Death Discov.* **2024**, *10*, 258.

[32] Kuo, W. T.; Zuo, L.; Odenwald, M. A.; Madha, S.; Singh, G.; Gurniak, C. B.; Abraham, C.; Turner, J. R. The tight junction protein

ZO-1 is dispensable for barrier function but critical for effective mucosal repair. *Gastroenterology* **2021**, *161*, 1924–1939.
[33] Chen, Y. N.; Hu, M. R.; Wang, L.; Chen, W. D. Macrophage M1/M2 polarization. *Eur. J. Pharmacol.* **2020**, *877*, 173090.
[34] Wen, H.; Li, L. Q.; Ge, X. Y.; Fei, Y.; Li, Y. A.; Li, M. H.; Xiao, W. D.; Luo, Z. Hydrogel-based artificial mucosa restores local immune and microbial homeostasis for treating ulcerative colitis. *Adv. Funct. Mater.* **2023**, *33*, 2212566.
[35] Seyedizade, S. S.; Afshari, K.; Bayat, S.; Rahmani, F.; Momtaz, S.; Rezaei, N.; Abdolghaffari, A. H. Current status of M1 and M2 macrophages pathway as drug targets for inflammatory bowel disease. *Arch. Immunol. Ther. Exp.* **2020**, *68*, 10.
[36] Bisgaard, T. H.; Allin, K. H.; Elmahdi, R.; Jess, T. The bidirectional risk of inflammatory bowel disease and anxiety or depression: A systematic review and meta-analysis. *Gen. Hosp. Psychiatry* **2023**, *83*, 109–116.
[37] Danduga, R. C. S. R.; Kola, P. K. Elevated plus maze for assessment of anxiety and memory in rodents. In *Neuroprotection: Method and Protocols*. Ray, S. K., Ed.; Human: New York, 2024; pp 93–96.
[38] Wang, Y. Y.; Zhou, Y. H.; Wu, Q. Y.; Li, Y. S.; Huang, Y. L.; Yu, K. X.; Li, P.; Lv, Z. Y.; Liu, H. T.; Zou, H. et al. Honeysuckle-derived nanovesicles regulate gut microbiota for the treatment of inflammatory bowel disease. *Adv. Sci.* **2025**, *12*, e05208.
[39] Ni, J.; Wu, G. D.; Albenberg, L.; Tomov, V. T. Gut microbiota and IBD: Causation or correlation. *Nat. Rev. Gastroenterol. Hepatol.* **2017**, *14*, 573–584.
[40] Kharaghani, A. A.; Harzandi, N.; Khorsand, B.; Rajabnia, M.; Kharaghani, A. A.; Houri, H. High prevalence of mucosa-associated extended-spectrum β-lactamase-producing *Escherichia coli* and *Klebsiella pneumoniae* among Iranain patients with inflammatory bowel disease (IBD). *Ann. Clin. Microbiol. Antimicrob.* **2023**, *22*, 86.
[41] Gao, P. Y.; Pang, S. Y.; Tang, Y. Q.; Wang, Q. Q.; Li, Q. Y.; Zhang, W. J.; Nie, C. X.; Niu, J. L.; Lian, K. X. Alterations in serum immune parameters, cytokines, intestinal permeability, fecal microbiota, and short-chain fatty acids in healthy and diarrheic suckling calves. *Agriculture* **2025**, *15*, 2289.
[42] Koyama, K.; Akiyama, R.; Oda, H.; Komiya, T.; Gokita, K.; Sako, T.; Mori, A. Effect of commercial prescription diets containing prebiotics on clinical signs and fecal miocrobiome in dogs with intestinal disease. *Pol. J. Vet. Sci.* **2024**, *27*, 599–610.
[43] Mirsepasi-Lauridsen, H. C.; Vester-Andersen, M.; Sørensen, N.; Krogfelt, K. A.; Bendtsen, F.; Petersen, A. M. The intestinal dysbiosis found in IBD-patients are linked to colonization with extra-intestinal pathogenic *Escherichia coli*. *Gastroenterology* **2017**, *152*, S632.
[44] Li, X. F.; He, N. N.; Wang, H. Y.; Wu, Z. N.; Wang, M. M.; Liang, H. W.; Xiao, L.; Yang, Z. Z.; Li, C. Y.; Xu, P. et al. Therapeutic effect of *Faecalibacterium longum* CM04-06 on DSS-induced ulcerative colitis in mice. *J. Appl. Microbiol.* **2025**, *136*, lxaf119.
[45] Lobatón, T.; Hoffman, I.; Vermeire, S.; Ferrante, M.; Verhaegen, J.; Van Assche, G. *Aeromonas* species: An opportunistic enteropathogen in patients with inflammatory bowel diseases. *A single center cohort study. Inflamm. Bowel Dis.* **2015**, *21*, 71–78.
[46] Chen, H. R.; Sun, Y.; Zhao, H. D.; Qi, X. F.; Cui, H.; Li, Q. M.; Ma, Y. α-lactalbumin peptide Asp-Gln-Trp alleviates hepatic insulin resistance and modulates gut microbiota dysbiosis in high-fat diet-induced NAFLD mice. *Food Funct.* **2022**, *13*, 9878–9892.
[47] Gan, L. Y.; Han, J.; Li, C. Y.; Tang, J.; Wang, X. B.; Ma, Y.; Chen, Y. F.; Xiao, D. G.; Guo, X. W. Tibetan highland barley fiber improves obesity and regulates gut microbiota in high-fat diet-fed mice. *Food Biosci.* **2023**, *53*, 102620.
[48] Peng, J.; Li, X.; Zheng, L.; Duan, L. F.; Gao, Z. X.; Hu, D.; Li, J.; Li, X. F.; Shen, X. C.; Xiao, H. T. Ban-Lan-Gen granule alleviates dextran sulfate sodium-induced chronic relapsing colitis in mice via regulating gut microbiota and restoring gut SCFA derived-GLP-1 production. *J. Inflamm. Res.* **2022**, *15*, 1457–1470.
[49] Li, X.; Wang, Q.; Wu, D.; Zhang, D. W.; Li, S. C.; Zhang, S. W.; Chen, X.; Li, W. The effect of a novel anticonvulsant chemical Q808 on gut microbiota and hippocampus neurotransmitters in pentylenetetrazole-induced seizures in rats. *BMC Neurosci.* **2022**, *23*, 7.
[50] Li, Y. M.; Li, L.; Tian, J. H.; Zheng, F. X.; Liao, H.; Zhao, Z. A.; Chen, Y. Y.; Pang, J. X.; Wu, T. Insoluble fiber in barley leaf attenuates hyperuricemic nephropathy by modulating gut microbiota and short-chain fatty acids. *Foods* **2022**, *11*, 3482.
[51] Li, A. L.; Ni, W. W.; Zhang, Q. M.; Li, Y.; Zhang, X.; Wu, H. Y.; Du, P.; Hou, J. C.; Zhang, Y. Effect of cinnamon essential oil on gut microbiota in the mouse model of dextran sodium sulfate-induced colitis. *Microbiol. Immunol.* **2020**, *64*, 23–32.
[52] Saudi, W. S. W.; Sjöblom, M. Short-chain fatty acids augment rat duodenal mucosal barrier function. *Exp. Physiol.* **2017**, *102*, 791–803.
[53] Hong, C. J.; Chen, S. Y.; Hsu, Y. H.; Yen, G. C. Protective effect of fermented okara on the regulation of inflammation, the gut microbiota, and SCFAs production in rats with TNBS-induced colitis. *Food Res. Int.* **2022**, *157*, 111390.
[54] Rattigan, R.; Lawlor, P. G.; Cormican, P.; Crespo-Piazuelo, D.; Cullen, J.; Phelan, J. P.; Ranjitkar, S.; Crispie, F.; Gardiner, G. E. Maternal and/or post-weaning supplementation with *Bacillus altitudinis* spores modulates the microbial composition of colostrum, digesta and faeces in pigs. *Sci. Rep.* **2023**, *13*, 8900.
[55] Bernad-Roche, M.; Bellés, A.; Grasa, L.; Casanova-Higes, A.; Mainar-Jaime, R. C. Effects of dietary supplementation with protected sodium butyrate on gut microbiota in growing-finishing pigs. *Animals* **2021**, *11*, 2137.
[56] Xu, J. J.; Wang, R. Y.; Liu, W. B.; Yin, Z. W.; Wu, J. R.; Yu, X.; Wang, W.; Zhang, H. T.; Li, Z. T.; Gao, M. J. et al. The specificity of ten non-digestible carbohydrates to enhance butyrate-producing bacteria and butyrate production *in vitro* fermentation. *Food Sci. Human Wellness* **2023**, *12*, 2344–2354.
[57] Peng, X.; Wei, Y. S.; Gong, D. M.; Zhang, G. W. Modulatory role of hesperetin-copper (II) on gut microbiota in type 2 diabetes mellitus mice. *Foods* **2025**, *14*, 2390.
[58] Ali, Q.; Ma, S.; Farooq, U.; Liu, B. S.; Wang, Z. C.; Sun, H.; Cui, Y. L.; Li, D. F.; Shi, Y. H. Chronological dynamics of the gut microbiome in response to the pasture grazing system in geese. *Microbiol. Spectr.* **2024**, *12*, e04188–23.
[59] Bajic, D.; Niemann, A.; Hillmer, A. K.; Mejias-Luque, R.; Bluemel, S.; Docampo, M.; Funk, M. C.; Tonin, E.; Boutros, M.; Schnabl, B. et al. Gut microbiota-derived propionate regulates the expression of Reg3 mucosal lectins and ameliorates experimental colitis in mice. *J. Crohn's Colitis* **2020**, *14*, 1462–1472.
[60] Pace, A.; Dipineto, L.; Fioretti, A.; Hochscheid, S. Loggerhead sea turtles as sentinels in the western Mediterranean: Antibiotic resistance and environment-related modifications of gram-negative bacteria. *Mar. Pollut. Bull.* **2019**, *149*, 110575.
[61] Holani, R.; Bar-Yoseph, H.; Krekhno, Z.; Serapio-Palacios, A.; Moon, K. M.; Stacey, R. G.; Donald, K. A.; Deng, W. Y.; Bressler, B.; Magaña, A. A. et al. Bile acid-induced metabolic changes in the colon promote Enterobacteriaceae expansion and associate with dysbiosis in Crohn's disease. *Sci. Signal* **2024**, *17*, eadl1786.
[62] Bondi, H.; Bortolotto, V.; Canonico, P. L.; Grilli, M. Complex and regional-specific changes in the morphological complexity of GFAP$^+$ astrocytes in middle-aged mice. *Neurobiol. Aging* **2021**, *100*, 59–71.
[63] Ohsawa, K.; Imai, Y.; Kanazawa, H.; Sasaki, Y.; Kohsaka, S. Involvement of Iba1 in membrane ruffling and phagocytosis of macrophages/microglia. *J. Cell Sci.* **2000**, *113*, 3073–3084.

[64] Feng, P. S.; Li, Q. Q.; Liu, L.; Wang, S. Y.; Wu, Z. P.; Tao, Y.; Huang, P.; Wang, P. Crocetin prolongs recovery period of dss-induced colitis via altering intestinal microbiome and increasing intestinal permeability. *Int. J. Mol. Sci.* **2022**, *23*, 3832.

[65] Bhandari, D.; Kachhap, S.; Madhukar, G.; Adepu, K. K.; Anishkin, A.; Chen, J. R.; Chintapalli, S. V. Exploring GPR109A receptor interaction with hippuric acid using MD simulations and CD spectroscopy. *Int. J. Mol. Sci.* **2022**, *23*, 14778.

[66] Zheng, Y. M.; Zhao, F. F.; Hu, Y.; Yan, F.; Tian, Y.; Wang, R. L.; Huang, Y. Y.; Zhong, L. Y.; Luo, Y. M.; Ma, Q. F. LC-MS/MS metabolomic profiling of the protective butylphthalide effect in cerebral ischemia/reperfusion mice. *J. Stroke Cerebrovasc. Dis.* **2023**, *32*, 107347.

[67] Chen, Y.; Shui, M. J.; Li, H. Y.; Guo, M.; Yuan, Q.; Hao, W.; Wang, T.; Zhou, H. F.; Chen, Z. J.; Wang, S. P. Inflammation-targeted delivery of probiotics for alleviation of colitis and associated cognitive disorders through improved vitality and colonization. *Biomaterials* **2025**, *318*, 123163.

[68] Cao, Y. N.; Fan, X. X.; Zang, T. Z.; Li, Y. T.; Tu, Y. M.; Wei, Y.; Bai, J. B.; Liu, Y. Q. Gut microbiota causes depressive phenotype by modulating glycerophospholipid and sphingolipid metabolism via the gut-brain axis. *Psychiatry Res.* **2025**, *346*, 116392.

[69] Cheng, J. Z.; Hu, H. K.; Ju, Y. M.; Liu, J.; Wang, M.; Liu, B. S.; Zhang, Y. Gut microbiota-derived short-chain fatty acids and depression: Deep insight into biological mechanisms and potential applications. *Gen. Psychiatry* **2024**, *37*, e101374.

[70] Lan, Z. F.; Yao, W.; Xie, Y. C.; Chen, W. S. S.; Zhu, Y. Y.; Chen, J. Q.; Zhou, X. Y.; Huang, J. Q.; Wu, M. S.; Chen, J. X. Oral troxerutin alleviates depression symptoms in mice by modulating gut microbiota and microbial metabolism. *Mol. Nutr. Food Res.* **2024**, *68*, 2470007.

[71] Wei, F. H.; Xie, W. Y.; Zhao, P. S.; Ji, Z. H.; Gao, F.; Chen, C. Z.; Zhang, Z.; Gao, W.; Yuan, B. Crataegus pinnatifida polysaccharide alleviates DSS-induced colitis in mice by regulating the intestinal microbiota and enhancing arginine biosynthesis. *Phytomedicine* **2025**, *142*, 156794.

[72] Wang, X. Y.; Wang, S. Q.; Zheng, B. D.; Guo, Z. B. Lotus seed starch-chlorogenic acid complexes alleviated chronic colitis and linked cognitive dysfunction via gut microbiota regulation: Gut-brain-axis interaction. *Carbohydr. Polym.* **2025**, *368*, 124158.

This is an open access article under the terms of the Creative Commons Attribution 4.0 International License (CC BY 4.0, https://creativecommons.org/licenses/by/4.0/).

© The Author(s) 2026. Published by Tsinghua University Press.